Order Number 9207139

Light scattering at the nonequilibrium crystal melt interface: Salol and succinonitrile

Williams, Lloyd Melvyn, Ph.D.

City University of New York, 1991

U·M·I
300 N. Zeeb Rd.
Ann Arbor, MI 48106

A

LIGHT SCATTERING AT THE NONEQUILIBRIUM CRYSTAL MELT INTERFACE: SALOL AND SUCCINONITRILE

by

LLOYD M.WILLIAMS

A dissertation submitted to the Graduate Faculty in Physics in partial fulfillment of the requirements for the degree of Doctor of Philosophy, the City University of New York.

1991

This manuscript has been read and accepted for the Graduate Faculty in Physics in satisfaction of the dissertation requirement for the degree of Doctor of Philosophy.

July 31, 1991
Date

Chair of Examining Committee

Aug 5, 1991
Date

Executive Officer

P. Wilzius

O. Martin

R. Giannetta

A. Genack

Supervisory Committee

The City University of New York

Abstract

LIGHT SCATTERING AT THE NONEQUILIBRIUM CRYSTAL MELT INTERFACE: SALOL AND SUCCINONITRILE

by

Lloyd Williams

Adviser: Professor Herman Cummins

The phenomenon of diffusive dynamic light scattering at the crystal-melt interface has been investigated in salol and succinonitrile. The origin of this phenomena is a matter of some controversy which this thesis will attempt to resolve. Of the several models that have been proposed to explain the phenomenon, the microbubble model (Cummins *et al.* Solid State Communications 60, p857 1986) and the mesophase model proposed by the ETH Zurich group of J. Bilgram and co-workers (Boni *et al.* Phys. Rev. A 28, p2953 1983) are the only two explanations still consistent with most of the observed properties of the scattering.

In the experiments on salol the scattering has been observed for 14 days. The hydrodynamic radius deduced from intensity correlation data increased continuously from $\sim$ 1 to 100 μm. When the scattering layer was trapped by the advancing crystal front, microscopic observation revealed bubbles as inclusions whose size agreed with the light scattering values.

In the experiments on succinonitrile the angular dependence of the scattered light was investigated. In the mesophase model the light is scattered by density fluctuations. The angular dependence of light scattered by density fluctuation is described by the Ornstein-Zernike form $I(q) = I_0(1+q^2\xi^2)$. However, light scattered by bubbles can be modeled using the appropriate Mie function for the problem. The

data was found to be incompatible with the Ornstein-Zernike form; however, it could be reasonably well fit by Mie theory.

The behavior of the onset of the scattering was also investigated, and it was found that the product $R_0 t_0 v_g^2$ was a constant, where R_0 is the onset radius, t_0 is the onset time, and v_g is the crystal growth velocity. This was consistent with the analysis of Mesquita *et al.*(1987) in which the onset of the scattering was modeled by considering the rate of buildup of dissolved gas at the advancing crystal-melt interface.

The gases dissolved in our samples of succinonitrile were identified by mass spectroscopy and found to have a composition similar to air.

ACKNOWLEDGMENTS

I would like to thank my research mentor Herman Cummins for his guidance and support during the course of my studies at City College. I would also like to thank several members of the faculty and staff here at CCNY for their assistance with various aspects of this work. I am particularly grateful to Professor Robert Graff for the mass spectrometer experiment performed in his laboratory to identify the gases dissolved in succinonitrile, and to Jack Downey for help with the photomicroscopy of the microbubbles. Others I would like to thank are: Jeffrey Bromberger in the Science Division computer facility, Marcelo Orellana and Victor Mae in the physics department electronics shop, Joe Altman and the machine shop staff, and Hugo Shimatz in the glass blowing shop.

I wish to acknowledge my predecessor Oscar Mesquita, from whom I inherited this experiment. His continued interest has been most valuable. Also I thank Martin Muschol who participated in the early stages of these experiments

I would also like to thank Professors Birman, Sarachik, Dine, Lindenbaum and Lax for the physics they taught me during my course work at CCNY, and Professor Tom Haines for an introduction to Biochemistry during the work on the osmotic properties of vesicles, which was my first project here at CCNY.

I would also like thank: Jean-Claude Toledano, Wim Van Sarloos, Yin Yeh, A Chernov and Andy Acrivos, for helpful discussions, and David Balzarini for teaching me photon correlation spectroscopy.

I am grateful to Peter Barber for providing the computer program that was used to calculate the Mie coefficients.

I would like to thank all the members of the light scattering group: NongJian Tao, Xiaoke Chen, Gen Li, Weimin Du, Dongning Lui, WinKee Lee, Henry Chou, Tarlok Aurora and Tracey Turner, for providing such a pleasant working atmosphere. I would Particularly like to thank Martin Muschol and Chester Qian for many useful

discussions and suggestion at lunch time walking over to Hank's, and in general for their good comradeship. Similarly, I would like to thank Chris Rutkowski for his friendship, and practical suggestions and help.

I thank all the member of my thesis committee: Pierre Wiltzius, Olivier Martin, Russ Giannetta and Azriel Genack for their guidance and help.

I would also like to express my thanks to several members of my family. I am deeply indebted to my father-in law for willingly let his wife be away from him for such a long period of time. My wife and I are extremely grateful to my mother-in law for taking primary responsibility of looking after our son Keith and daughter Shail, enabling me to complete this thesis and my wife to complete her practical training.

I thank Keith and Shail for giving me inspiration to keep going through the ups and downs of a Ph.D.

Lastly, but most importantly, I owe a great debt of gratitude to my wife Urmil for her love and patience during the entire process.

TABLE OF CONTENTS

TABLE OF FIGURES

TABLE OF TABLES

1. INTRODUCTION

1.1. Overview

The subjects of crystal growth and bubble nucleation are of wide technical interest. The need to grow large high purity crystals for applications in the semiconductor and optics industries has provided an impetus for much research in the field of crystal growth. The nucleation of gas bubbles is important in many fields[1] varying from the operation of hydrogen bubble chambers, and the degasification of steel, to the formation of plastic foams and the production of beer and soft drinks. Bubble nucleation is also important in the field of crystal growth, as bubbles often become trapped impurities in melt grown crystals. This leads to a degradation of the electrical and optical properties of the crystals. This common occurrence was reviewed by Wilcox and Kuo[2]. Figs. 1.1(a-d) give some examples, quoted in their review, of bubbles trapped in crystals. Fig 1.1(a) is taken from Powers[3] and shows fjord-like inclusions of air in sucrose crystals. Fig 1.1(b) is taken from Pollock[4] and shows lines of 1μm microbubbles in sapphire grown by an edge defined film fed technique. Fig 1.1(c) is taken from Nassau and Broyer[5] and shows bubbles included in calcium tungstate crystals, grown by the Czochralski Method. Fig 1.1(d) is taken from Sugii *et al.*[6] and shows a stream of bubbles down the center of a crystal of lead germanium oxide, again grown by the Czochralski Method. These examples of bubble formation have arisen as a result of heterogeneous nucleation, which is a poorly understood process. Most theoretical work in this field considers mainly homogeneous nucleation.[7-13] There is frequently a large discrepancy between the necessary conditions for nucleation predicted by theory and those found by experiment. In particular one generally finds that the gas supersaturations necessary to form bubbles are far below those predicted by theory[14,15]. However, it is expected that crystal surfaces could play an important role in facilitating the nucleation process for two

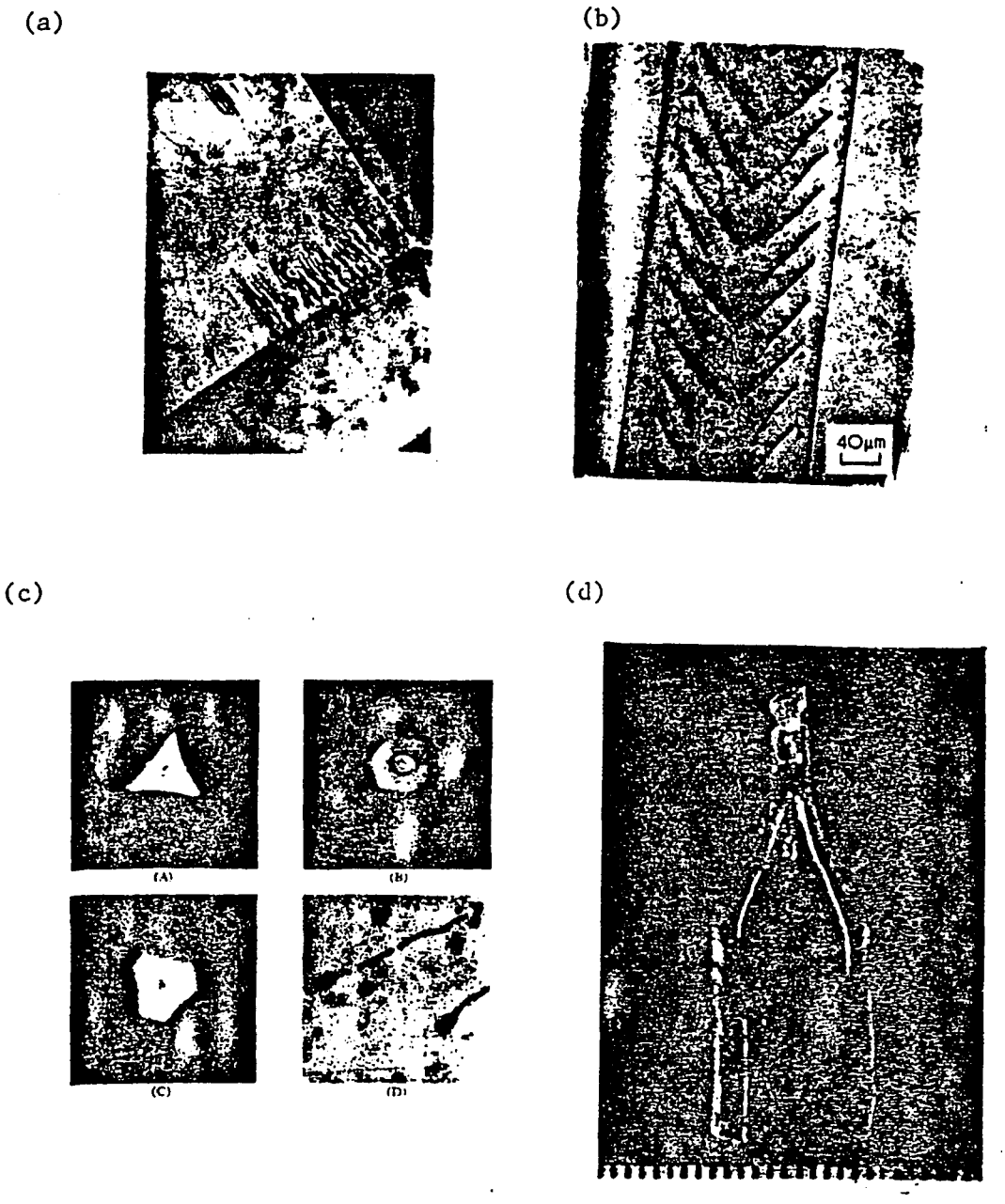

Fig 1.1: Examples of bubbles included in crystal. ((a) is taken from Powers[3] and shows fjord like inclusions of air in sucrose crystals, and is reprinted by permission from NATURE vol 13 pp716 1958. (b) is taken from Pollock[4] and shows lines of 1μm microbubbles in sapphire, and is reprinted by permission from The Journal of Material Science vol 7 pp639 1972. (c) is taken from Nassau and Broyer[5] shows bubbles include in calcium tungstate crystals, and is reprinted by permission from The Journal of Applied Physics vol33 pp3067 1962. (d) is taken from Sugii *et al.*[6] and shows a stream of bubbles down the center of a crystal of lead germanium oxide, and is reprinted by permission of The Journal of Crystal Growth.)

reasons: firstly, the gaseous impurities that constitute the bubbles are segregated at the interface by solute rejection as the crystal grows, and secondly, the various cracks, defects, steps, and ledges, grain boundaries of the crystal surface provide preferred sites for the nucleation.[15,16]

Dynamic light scattering provides a useful noninvasive technique to investigate the dynamics at the interface as the crystal grows. We find that it is possible to probe not only the motion of the bubbles at the interface, but also in certain cases the actual growth mechanism of the crystal.

Our interest in these phenomena began with the discovery in 1978, by H. Guttinger *et al.*[17], at the ETH in Zurich of a new, and at that stage unexplained, source of intense light scattering at the crystal-melt interface. A laser beam incident on the horizontal interface between an ice crystal and highly purified water in a zone-refining apparatus initially produced virtually no scattering. But when growth was initiated by driving the sample tube downwards at speeds exceeding 1.5 μm/s, intense quasielastic light scattering appeared at the interface after an initial onset time on the order of one hour. The intensity autocorrelation function of the scattered light was found to be exponential, with a decay rate Γ (corresponding to the optical linewidth) that scaled with q^2, which is characteristic of relaxational (diffusive) processes; i.e. $\Gamma=Dq^2$ where D is an effective diffusion constant, and q is the scattering vector ($q=2k_i \sin \theta/2$ where k_i is the incident wave vector).

1.2. Description of the Basic Light Scattering Phenomena

Since the initial discovery, this phenomenon (or phenomena) has been observed in a total of eight different materials, as shown in Table 1.1, in experiments performed at the ETH-Zurich[17-35], City College of New York (CCNY)[36-40], the University of California-Davis[41-43], the University of Minas Gerais (Brazil)[44-46] and the CNET laboratory in France[47-49]. There are actually two quite different effects observed in materials which are strongly faceted. We shall refer to the two types of scattering as

Material	Diffusion Coefficient (cm^2/sec)	Radius (μm)
Benzophenone[46]	$\sim 1\times10^{-10}$	~ 2
Biphenyl[44]	$\sim 4.9\times10^{-10} - 1.5\times10^{-9}$	1.0 - 3.6
Cyclohexane[33]	6×10^{-9}	0.26
Cylcohexanol[39]	$2\times10^{-11} - 9\times10^{-11}$	0.34 – 1.5
Naphthalene[44]	$1.6\times10^{-10} - 1.3\times10^{-9}$	1.7 – 8.2
Salol a-axis[29]	$7.5\times10^{-10} - 1.25\times10^{-9}$	0.22 – 0.36
a-axis[37]	$0.6\times10^{-10} - 1.0\times10^{-10}$	2.7 – 4.6
b-axis[37]	$1.0\times10^{-10} - 1.0\times10^{-9}$	0.27 – 2.7
b-axis[40]	$2.3\times10^{-12} - 7.8\times10^{-10}$	0.35 – 117.0
Succinonitrile*	$3.6\times10^{-10} - 4.5\times10^{-9}$	0.4 – 5.0
Succinonitrile[47]	$1.5\times10^{-9} - 3.0\times10^{-9}$	0.6 – 1.2
degassed[47]	$2.9\times10^{-11} - 6.9\times10^{-11}$	31.0 – 52
Water a-c axis[42]	$1.5\times10^{-11} - 3\times10^{-9}$	0.3 – 65
c-axis[28]	$1.4\times10^{-8} - 5.7\times10^{-8}$	0.019 – 0.079
c-axis[42]	$4.5\times10^{-9} - 6.3\times10^{-9}$	0.059 – 0.072
D_20[21]	(close to H_20 values)	

Table 1.1: Diffusion coefficients and corresponding radii from boundary layer light scattering measurements (* values quoted in this thesis).

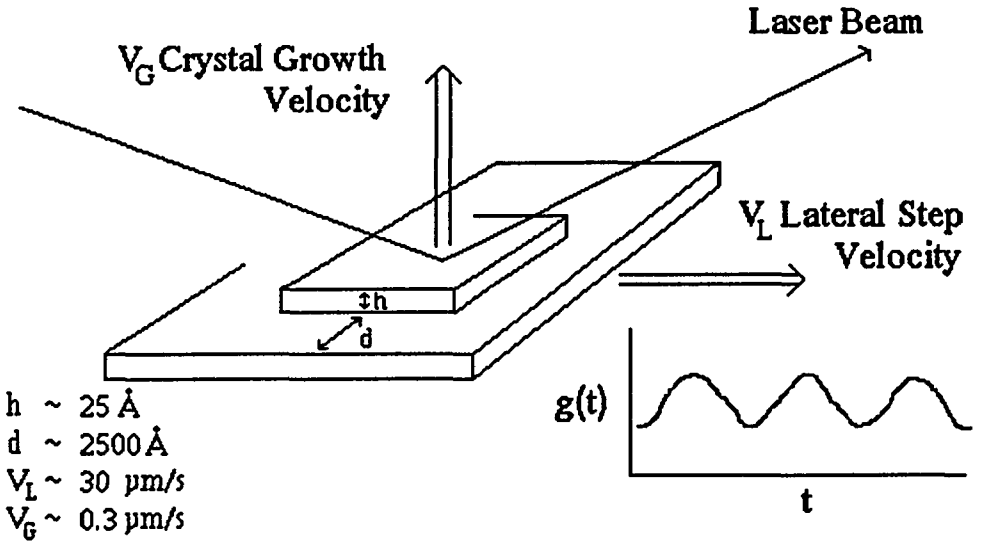

Fig 1.2: Sketch of growth steps on face of crystal that give rise to oscillatory scattering

oscillatory and diffusive. They may coexist and be observed simultaneously on the surface of faceting materials, but are two quite distinct phenomena in terms of their origin.

The oscillatory scattering is caused by the scattered light being Doppler shifted by growth steps propagating across the surface of the crystal[36, 37]. This frequency-shifted scattered light beats with the unshifted scatted light and gives the oscillatory correlation functions observed in salol and benzophenone.

The intensity correlation function can be fitted to

$$c(t) = B + A \cos(\omega t)$$

$$\omega = \mathbf{v}_l \cdot \mathbf{q}_{||}$$

where $\mathbf{v}_l$ is the lateral velocity of the growth steps and $\mathbf{q}_{||}$ is the component of the scattering vector $\mathbf{q}$ parallel to the interface. This is illustrated in Fig 1.2. Unlike the oscillatory correlation functions observed in scattering from capillary waves on fluid surfaces, these oscillations are not damped. The main properties of this scattering are that[29, 36, 37, 46]:

a) it starts up immediately after the crystal begins to grow

b) it is much weaker than the diffusive scattering.

c) it is highly anisotropic, displaying Bragg peaks at scattering angles at which $\mathbf{q}_{||}$ is normal to one of the growth faces.

This scattering has been seen in Salol[29, 36, 37] and benzophenone[46].

The origin of the diffusive scattering constitutes a controversy which this thesis will attempt to resolve. It is primarily characterized by an exponentially decaying correlation function. It is also usually much more intense than the oscillatory scattering. Experiments by Mesquita *et .al.*[36, 37] on salol (at CCNY) showed that these two scattering processes occur simultaneously, and can be separated by appropriate choices of wave-vector and polarization directions.

This diffusive scattering phenomenon, as revealed by the experiments to be described below, has the following basic properties :

a) It occurs in a fluid boundary layer at least several microns in thickness, and in salol and benzophenone co-exists with the translational dynamics seen on the crystal surface.

b) It is much stronger than scattering from either the crystal surface or the bulk fluid.

c) It requires an onset time on the order of hours to begin, which is increased by prolonged degasification of the sample.

d) The intensity correlation function of the scattered light is approximately exponential with a polydispersity that varies in some experiments from a small value at onset to a value on the order of unity after prolonged growth.

e) It occurs on both atomically smooth and rough interfaces.

f) The effective diffusion constant D is typically 10^4 times smaller than the molecular self-diffusion coefficient, and 10^6 times smaller than the thermal diffusion coefficient of normal liquids.

g) It can persist for many hours after growth has stopped.

h) The scattering layer can lift off of the interface if the crystal is melted back quickly.

Several models have been proposed to explain the origin of this diffusive scattering:

1) Capillary waves on the interface (Bilgram *et al.*).[18]

2) Diffusion of defects in the surface (Keizer *et al.*).[50-52]

3) Partial orientation of molecules in the liquid layer adjacent to the interface (Mesquita *et al.*).[36]

4) Dynamic roughening (van Saarloos and Gilmer).[38]

5) A new mesophase (Boni *et al.*).[28]

6) Gaseous microbubbles (Cummins *et al.*).[38]

Models (1) - (4) are now generally regarded as inconsistent with various elements of the experimental data, particularly the observed thickness of the scattering layer which increases with decreasing growth velocity.[32] Thus the mesophase model 5) and the gaseous microbubble model 6) are currently the only extant models consistent with the basic properties (a-h) given above.

1.3. Review of Previous Experiments

1.3.1. Ice-water Experiments of the ETH Group

Anomalous dynamic light scattering at the crystal-melt interface was first observed by Bilgram, Güttinger and Känzig, at the ETH in Zurich.[18] Their experiments were performed on ice crystals growing along the c-axis in a zone refining apparatus placed in a cold room at -18°C. In this experiment it was found that after the initiation of growth and the formation of the basal plane on the top of the growing crystal, light scattering could be observed when a critical velocity v_c of 1.5 μm/s was exceeded, after an onset time of about one hour. The intensity correlation function of

the scattered light was found to be accurately a single exponential with a corresponding linewidth Γ of about 2,000 rad/sec at a scattering angle of 90°. This would correspond to scattering from objects with a hydrodynamic radius R_h of about 25 nm. The scattering was found to exhibit hysteresis, that is once the scattering had been initiated it persisted even if the growth velocity dropped below v_c. The scattering was only seen to disappear sometime after the growth was completely stopped or when the interface was melted away. Γ was found to have the same linear dependence on q^2 whatever the growth rate. The authors proposed that the scattering was caused by a fluctuating corrugated interface (i.e., overdamped capillary waves). In this model the decay time of a Fourier component with wave vector q could be calculated from the Gibbs-Thomson equation.

A preliminary version of these results had previously been reported in 1975.[17] In this preliminary paper, the diffusive scattering exhibited two simultaneous decay rates, one fast and one slow. The process observed in Ref. (18) corresponded to the fast decay rate. The slow decay rate process was not seen in the later work of the ETH group, although it has been studied subsequently by Yeh and co-workers in California[41-43], as described below. It is a matter of some controversy whether these two decay rates correspond to two distinct phenomena. Vesenka and Yeh[42,43] have suggested that the slow component may correspond to the gaseous microbubble mechanism (5), while the fast component is intrinsic, produced by crystal formation from the melt.

In 1979 the ETH group[19] measured the dependence of the scattering intensity on the azimuthal angle θ and found it to be essentially independent of angle. Also, by studying the coherence properties of the scattered light, they were able to estimate that the scattering layer was less than 6μm thick.

In the first publications of the ETH group, it was assumed that the scattering process was two-dimensional, i.e. that it occurred in the planar interface between the

crystal and the melt. Experimentally, two-dimensional scattering can be distinguished from three-dimensional scattering by studying the effect of varying the polar angle ψ; for two-dimensional processes, the projection of the scattering vector on the plane determines the spectrum, while for three-dimensional processes, it is the total scattering vector which is important.

In a 1980 article Bilgram and Böni[20] measured the variation in the scattered intensity and linewidth with the polar angle ψ. Comparisons of linewidths at $\psi=65°$ and $\psi=90°$ revealed that the scattering process is three-dimensional. This conclusion was incompatible with the two-dimensional model of the corrugated interface and a new model was introduced to explain the scattering. In this model an intermediate

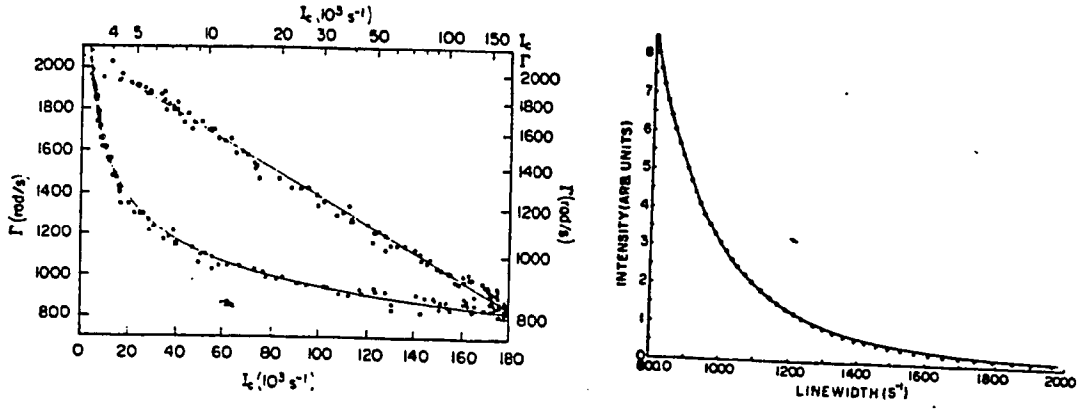

Fig 1.3: On the left, Linewidth of the scattered light vs the intensity in a linear plot (crosses and in a log-log plot squares. Solid lines are obtained by linear regression. Figure is taken from ref 28. On the right The dotted curve is the scattered intensity calculated by the Mie scattering program for spheres as a function of the linewidth of the transient diffusive scattering at a fixed angle of 90°. The continuous curve is the best fit of $I = B\ (6.61 \times 10^{-3}/\Gamma)$ to the Mie curve. The exponent obtained was $n=4.587$ resulting in $\Gamma \propto (I)^{-0.22}$. Figure taken from ref 44.

layer is assumed to form between the ice and water, and light is scattered by thermodynamic fluctuations in this layer. In order to investigate whether this phenomenon was peculiar to the ice-water system, other systems were investigated. In a short article in 1981[21] the ETH group reported that D_2O exhibited essentially the same scattering characteristics as H_2O.

In 1983 Böni, Bilgram and Känzig[28] reported a more complete study of the ice water system that revealed several interesting properties of the scattering. A Brillouin scattering study revealed that the increased scattering is due to the central Rayleigh component and that the intensities of the Brillouin components are unaffected. It was also found that the critical growth velocity increased with increasing temperature

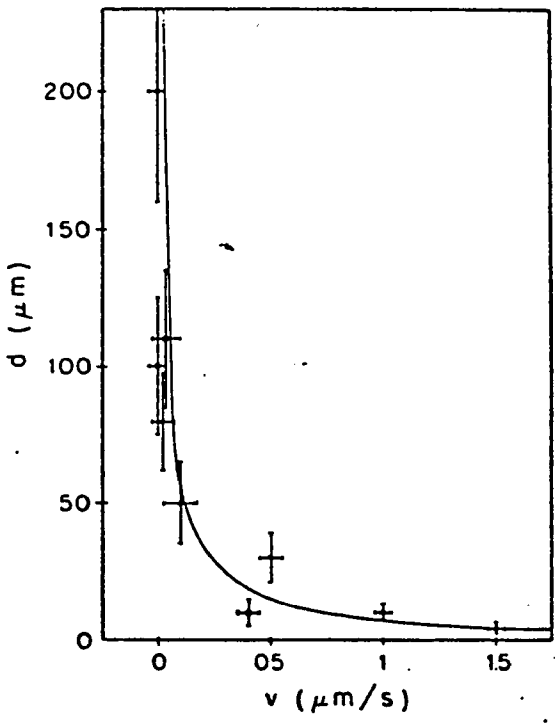

Fig 1.4: Thickness of the interface layer vs growth rate measured during slowing down (full dots) and a subsequent increase of the growth rate (open dots). (Figure taken from ref 32)

gradient in the ice. Measurements were made on the time dependence of the intensity and linewidth of the scattered light over a three hour period after the onset of scattering. The intensity I was seen to increase and the linewidth Γ to decrease with time. Γ was found to be related to I by a power law dependence: $\Gamma \propto I^{-\alpha}$, where $\alpha = 0.23 \pm 1\%$. It was stated that after this transient period both I and Γ are stationary, although no data was presented to support this statement. This is shown in Fig 1.3 along with Mesquita's fit of the data which is described in section 1.3.4.

In the discussion of these results the interface layer and corrugated interface models were compared. The corrugated boundary model was ruled out and the theory for the boundary layer model was discussed in more detail. From measurements of the intensity of the scattered light it was inferred that the boundary layer has an isothermal compressibility χ_T about 700 times larger than that of pure water. This large compressibility causes the usual entropy fluctuations responsible for the Rayleigh line in normal liquids to become stronger and narrower, somewhat resembling the characteristics of fluids near the critical point. From measurements of the linewidth it was inferred that the correlation length ξ of the fluctuations in the boundary layer is in the range $20 < \xi < 80$ nm.

In their 1988 study of the ice-water system[32], Bilgram and co-workers employed a Czochralski growth apparatus[17] with the water below the ice crystal rather than above it. The essential features of the scattering were found to be the same as described previously.[18, 19, 28] However, several new features were measured. For growth rates less than 1.5 μm/s the scattering layer was thick enough to be imaged and measured. The thickness of the layer d was measured as a function of v_g, and it was found that $d \propto v_g^{-1}$. This result is shown in Fig 1.4. After stopping growth the layer reached a thickness of 200 μm, and upon melting the scattering layer "lifted off" the interface and stayed back in the water. The Raman spectra of the scattering from the interface did not differ significantly from normal water. Although some small

differences in the intensity of the polarized Rayleigh wing and in the O-H stretching band were observed, the interface was described as "essentially water-like". From the different growth conditions relating to the previous zone-refining geometry it was concluded that the formation of the scattering layer does not depend on gravity.

1.3.2. Ice-water Experiments of the University of California Davis Group

The first confirmation of diffusive interfacial light scattering by investigators outside of Zurich came in the paper of Brown *et al.*[41] at the University of California Davis, in which scattering was seen in ice growing along the a-axis in a Bridgman growth apparatus. The linewidths reported in this work corresponded to a decay time ~ 3.5 times slower than that reported by the ETH group.[18,19]

In the California group's work on ice growing along the c-axis, both a fast and a slow component were reported. In this study several interesting features of the slow component were observed. It was noted that the slow component could be enhanced if high purity helium or argon was bubbled through the melt to saturate it. It was also reported that there was a deviation from the linear dependence of Γ on q^2. This was explained in terms of a phenomenological equation that includes both diffusion and fluctuations in the bubble concentration.

A "lift off layer" was observed in samples injected with helium, although not argon. When growth was stopped after scattering had begun and the crystal was melted back (by reversing the motor drive), the scattering layer was observed to remain stationary in the melt as the interface moved away. This effect was first seen by Mcdonaugh (unpublished data, 1985) and reported in a preliminary form in 1987.[43] It is interesting to note that helium very effectively enhances the scattering, since the ice crystals grown by the ETH group in the Czochralski apparatus[32] were subjected to an overpressure of about 100 mbar of helium. This was done because they asserted that helium is more soluble in ice than in water. The California group also reported that the polydispersity $Q(Q=\mu_2/<\Gamma^2>)$ increased with the hydrodynamic radius R_h. This was

especially observable in the gas-injected samples. In the Ph.D. thesis of Vesenka[43] it was noted that upon applying a significant overpressure to the melt, R_h was found to decrease.

1.3.3. Experiments on Salol and Cyclohexanol

From their initial experiments on the c-axis of the ice water system the ETH group switched to the highly faceting organic crystal salol (phenyl salicylate).[23] This investigation revealed two different scattering mechanisms. One was isotropic, characterized by an exponentially decaying correlation function similar to the scattering seen in water; the other was highly anisotropic characterized by an oscillatory correlation function. The oscillatory scattering had a critical growth velocity of 0.2 μm/s and began as soon as the crystal started growing. The diffusive scattering had a critical velocity of 0.4 μm/s and required about 2 hours for onset, at which time over the course of about 15 minutes the oscillatory correlation became damped and the exponential one emerged and dominated the scattering. The oscillatory scattering was interpreted as resulting from light being Doppler shifted by a scatterer moving parallel to the scattering vector with a velocity about 150 times greater than the crystal growth velocity.

The diffusive scattering in salol exhibited the same hysteresis as the scattering in the ice-water system; however the linewidth of the scattered light was 10-20 times smaller than the ice-water linewidth reported in Ref. (18) which corresponds to a hydrodynamic radius R_h of 0.25-0.5 μm. It was noted that this decay time agreed with the predictions of the Gibbs-Thomson equation of the model proposed in Ref. (18) even though that model did not take into account the three-dimensional nature of the scattering.

New observations on light scattering in salol were reported by the CCNY group in 1984.[36] By exploiting the birefringence of the crystal, they were able to separate the diffusive and oscillatory scattering and show that the two phenomena coexist at the

interface. It was suggested that moving growth steps on the faceted surface of the crystal Doppler shift the scatterred light causing the oscillatory scattering. Two growth mechanisms were considered to generate the steps: nucleated layer growth and screw dislocation growth. The predictions of the dependence of the growth rate v_g on undercooling ΔT were tested for both mechanisms, and it was established that for low growth rates the screw dislocation mechanism was dominant, although at higher growth rates nucleated layer growth seemed to play an important role.

The observed properties of the diffusive scattering were essentially the same as those reported by the ETH group.[23] A tentative model for the scattering based on the existence of some orientational ordering of the molecules at the interface was proposed.

In a subsequent article by the CCNY group, the occurrence of scattering on both the a and b face of salol was reported.[37] Scattering was also observed during melting, although at much higher velocities. The previously proposed model of orientational order was ruled out by a preliminary observation of scattering in cyclohexanol, which crystallizes in a plastic phase and therefore possesses no orientational order.

In 1984 Dürig, Bilgram and Känzig[29] reported a comprehensive study of the salol system. Both the oscillatory and diffusive scattering were investigated. They also interpreted the oscillatory scattering as due to growth steps originating from screw dislocation spirals. From measurements of the Bragg peaks in the scattered intensity, the spacing between steps d_o was shown to be typically 0.4 μm. From the period of the oscillations in the correlation function a typical lateral step velocity was v_l=40 μm/s. For growth along the b axis they found $d_o \propto v_l^{-1}$. The height of the steps h could also be determined. As $h=d_o(v_g/v_l)$, where v_g is the growth speed of the crystal, h was calculated to be about 6 nm or 2.5 lattice constants.

In their measurements of the diffusive scattering they reported seeing scattering only for growth along the a axis, in contrast to their earlier report[23] of scattering on

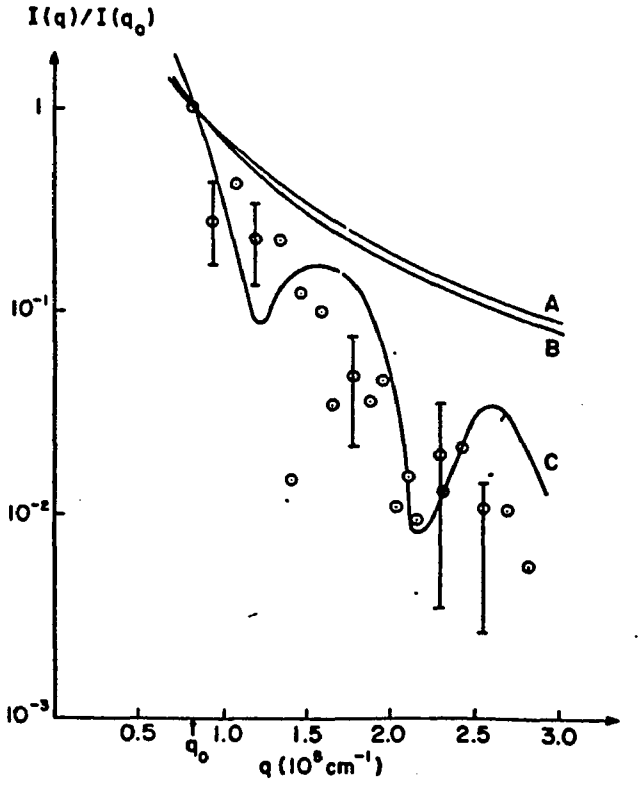

Fig 1.5: Intensity of scattered light vs scattering vector q in Salol. Data normalized to $I(q)/I(q_0) = 1$ at $q_0 = 0.825 \times 10^5$ cm $^{-1}$. The theoretical curves are (A) Ornstein-Zernike, ξ = 3,000 Å. (B) Ornstein-Zernike, absolute lower limit for $\xi = \infty$. (C) Mie scattering for spheres of radius R = 3,000 Å. Figure taken from ref 38.

both the a and b face. Their measurement of the linewidth Γ was in essential agreement with their earlier paper[23], and the origin of the scattering was assumed to be a mesophase boundary layer similar to the layer assumed to exist in the ice-water system.[28]

In 1986 the CCNY group[38] proposed the microbubble hypothesis for the scattering; this model will be outlined in section 2.3.1. Preliminary measurements of the angular dependence $I(\theta)$ in salol were also reported. It was found that $I(\theta)$ could be well fitted by Mie theory but that the intensity fell off too rapidly with scattering angle to be fitted with Ornstein-Zernike theory, even in the limit of infinite correlation length ξ. This result is shown in Fig 1.5.

A full report of the scattering in cyclohexanol was given in 1987 by the CCNY group.[39] These measurements gave a value for R_h in the range 0.6 - 3.0 μm. A "lift-off layer" similar to that observed by Yeh[42] and Bilgram[32] was also observed. The persistence of scattering long after growth had stopped was also noted, although unlike salol the relaxation time for the cyclohexanol interface to return to its equilibrium position is very short, ~ 10 sec. compared to ~ 20 hours for salol.

In a major review of dynamics at the solid-liquid transition[30] Bilgram developed the theory of the boundary layer, in which it was postulated that the creation of the "mesophase" is brought about by a non-equilibrium wetting transition. In the same article the microbubble hypothesis of Cummins *et al.*[38] was discussed and rejected, primarily on the grounds that the energy barrier to bubble nucleation ($e^{-\Delta F/k_BT}$ where ΔF is the energy of formation of a gas bubble) is prohibitive.

The first direct observation of the microbubbles was reported in 1990 by the CCNY group[40]. This experiment (on salol) is described in this thesis in Sec.4.1. The paper also described experiments in which the growth tube containing the crystal was connected to a vacuum station and the sample was subjected to pumping. In this experiment the scattering was seen to disappear after 24 hours of pumping. A preliminary force balance model along the lines of that proposed by Ladeira and Mesquita[46] was discussed as a possible mechanism for selection of the initial radius R_o. Comparisons were made with data from the experiments on salol and water.[28, 29, 37]

1.3.4. Biphenyl and Naphthalene Experiments of the Minas Gerais Group

Mesquita *et al.*[44] (in Brazil) observed scattering in two new materials, naphthalene and biphenyl. The R_h observed in these materials was also in the micron range. They too observed that smaller polydispersities corresponded to smaller radii. In this study the relationship between the time for the onset of scattering t_o and the radius at onset R_o was investigated. It was observed that the product $t_o R_o v_g^2$ was a constant for each material.

Mesquita *et al.*[44] also analyzed the data on the onset of scattering in the ice-water system reported by Boni *et al.*[28] They found that the experimental relationship between the linewidth Γ and the intensity I, $I \propto \Gamma^{-\alpha}$ could be modeled if the scatterers were assumed to be bubbles and the intensity I was given by Mie theory. The agreement in the values of α was quite good: Boni *et al.*[28](experiment) α=0.23, Mesquita *et al.*[44] (theory) α=0.22. This is shown in Fig 1.3.

The existence of a critical velocity for the onset of scattering has been reported by the ETH group[18,19, 28] for the ice water system. It appears that this may be a unique feature of this system. Mesquita and Ladeira[45] have suggested a mechanism based on the Rayleigh-Benard convective instability that might explain this phenomenon. While it is true that water is unique among the systems studied in having a negative thermal expansion in the temperature region around the freezing point, it is hard to see how this could explain the same critical velocity being observed by Bilgram in ice grown in a Czochralski apparatus[32] where the melt is stable against convective instabilities.

Ladeira and Mesquita have also observed oscillatory scattering in benzophenone[46] growing along the [110] direction. The scattering was assumed to also come from growth steps propagating out from screw dislocations. In the same work Mesquita[46] also suggested that force balance considerations could play a role in the selection of the initial radius.

In recent unpublished work Mesquita has repeated the onset measurements of Ref.44 on samples of naphthalene purified by vacuum sublimation, which then had argon bubbled through them. The expression $v_g^2 t_o R_o$ was again found to be a constant. A clear relationship between R_o and v_g was also noted.

Mesquita also measured $I(\theta)$ for the naphthalene sample and found a repeatable peak in the data at $\theta = 50°$. He notes that this peak is around the right position for the

Mie curve that corresponds to particles of roughly the same size as the size extracted from photon correlation spectroscopy, a strong indication that the scattering is due to bubbles. The time t_d for which the scattering persists after growth is terminated was measured and found to be proportional to $1/v_g^2$.

1.3.5. Succinonitrile Experiments of the Paris Group

Laherrere *et al.*[47] in Paris observed diffusive light scattering in the plastic crystal succinonitrile. The values of R_h were in the range 0.3-0.6 μm. The effect on the scattering of pumping on the melt was investigated. The crystal was melted and then recrystallized at room temperature. Any released gases were then pumped out. After 10 such cycles the scattered intensity was reduced by a factor of at least 4, and the onset radius was also seen to increase by a factor of 10. Laherrere *et al.*[48] have recently repeated this experiment and carefully studied the dependence of the initial radius R_o and onset time t_o on residual gas pressure and growth velocity. They also reported a preliminary attempt to identify the gas pumped out of the sample by infrared absorption spectroscopy[48]. This gas they identified as methanol, a material used in the manufacture of succinonitrile.[48] This group has also recently investigated the unstable crystal-melt interface in directional solidification of a binary system, and has shown that the light scattering spectrum is modified by the occurrence of a cellular instability.[49]

1.3.6. Cyclohexane Experiments of the ETH Group

In 1989 the ETH group initiated a new study of diffusive scattering in cyclohexane.[33] Cyclohexane was chosen because of the absence of a permanent dipole moment. Thus the possibility of some long range dipole-dipole interaction causing the scattering phenomena could be ruled out. Measurements of the linewidth Γ showed no departure from the q^2 behavior seen in the other materials, and corresponded to an R_h

of about 0.26 μm. The angular dependence I(θ) of the scattering intensity was measured, and found to fit the Ornstein-Zernike form. $I(q) \sim (1+q^2\xi^2)^{-1}$ with ξ=0.2 μm. This result is shown in Fig 1.6. It was stated that I(θ) could only be fitted by Mie theory for a broad size distribution of the form $N(\alpha) \sim \alpha^5$ with α, the Mie coefficient $1 < \alpha < 10$; such a distribution of sizes would have produced a large deviation from single exponential behavior in the correlation function which was not observed.

A new geometry was also used to observe scattering. A temperature sensor was embedded in a crystal that had been zone refined several times, and a 3 mm liquid sphere was melted in the crystal. When the heat source was removed, the sphere grew back inwards with velocities in the range 0-30 μm/s, considerably faster than the velocities obtained in the zone refining apparatus, and scattering was seen. The linewidth of the scattering was similar to the previous results, corresponding to a slightly larger R_h. The onset time for this geometry was extremely short, on the order of several seconds. If the growth was stopped and the crystal melted back, the interface layer followed the interface and did not "lift off".

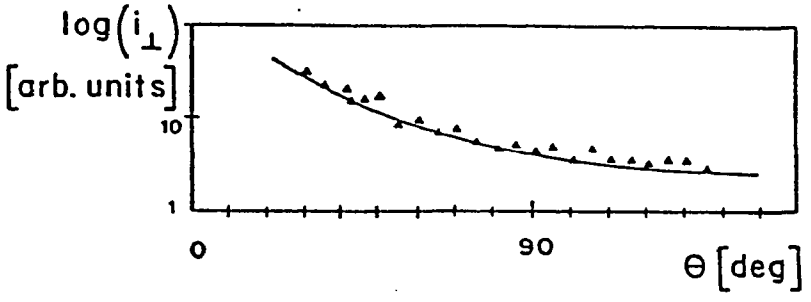

Fig 1.6: Angular Intensity Data. (from ref 33)

2. THEORY

2.1. Light Scattering Theory

2.1.1. Photon Correlation Spectroscopy

Photon correlation spectroscopy (PCS) is a technique that became possible in the early 1960's with the advent of the laser[54,55,56]. In PCS one examines the fluctuations in the intensity of scattered light caused by the slow dynamics of the scattering source. The width of the spectrum of the fluctuations is typically of the order of several kHz, too small to be resolved by conventional interferometric means. The spectrum is indirectly determined by measuring the intensity autocorrelation function of the scattered light, using a photon counting technique. This correlation function is related to the spectrum by Fourier transformation. What follows is a simplified outline of the derivation of the correlation function of light scattered from a system of diffusing bubbles. This derivation has been described in great detail in many places[54-58]. The treatment that follows is a condensed version of the derivation given in Berne and Pecora.[58] It makes many assumptions and approximations about the nature of the scatterers but contains the essential physics of PCS.

If we consider the system producing the scattering to be described by a local polarizability tensor $\alpha(\mathbf{r},t)$, then the electric field $E_s(\mathbf{R},t)$ at point $\mathbf{R}$ and time t, scattered by a fluctuation $\delta\alpha(\mathbf{r},t)$ can be written as

$$E_s(\mathbf{R},t) \propto e^{i(k_s \cdot r - i\omega t)}\, \delta\alpha_{is}(q,t) \tag{2.1}$$

where

$$\delta\alpha_{is}(q,t) = \sum_{j=1}^{N} \delta\alpha_{is}^{j}(q,t)\, e^{iq \cdot r_j(t)} \tag{2.2}$$

Here $\delta\alpha_{is}(\mathbf{r},t) = \mathbf{n_i} \cdot \underline{\underline{\alpha}}(\mathbf{r},t) \cdot \mathbf{n_s}$ is the inner product of the polarization tensor of the scatterer (bubble) with the incident and scattered polarization vectors (See Fig 2.1).

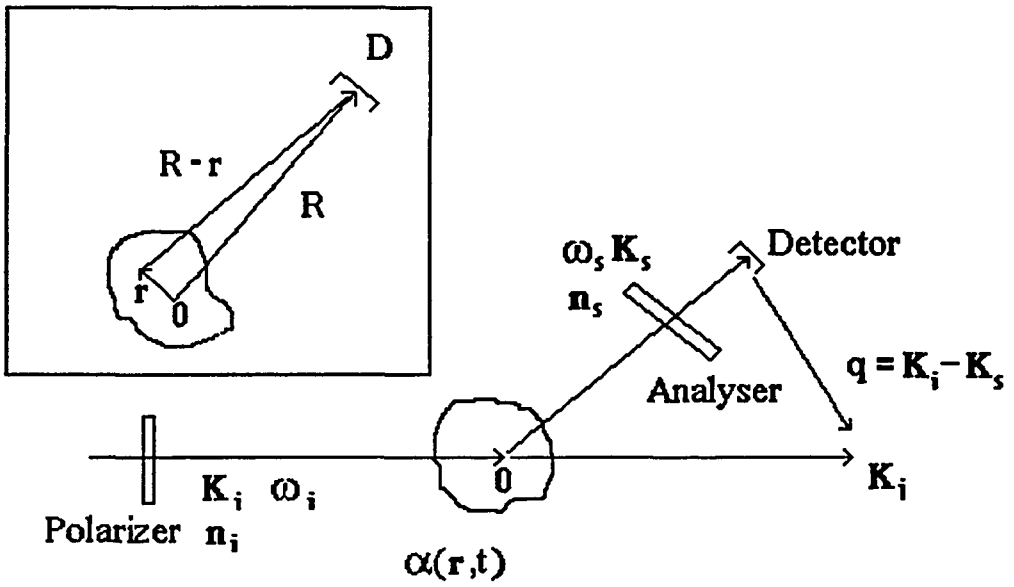

Fig 2.1: Sketch of scattering geometry of a typical light scattering experiment. $\mathbf{q} = \mathbf{k_i} - \mathbf{k_s}$ is the scattering vector. As the scattering is elastic $k_i = k_s$ then $q=2k_i \sin(\theta/2)$. The insert shows the definition of the spatial coordinates **r** and **R**.

The sum is over all scatterers in the illuminated volume. Thus, the time correlation function of the scattered field is

$$<E_s^*(\mathbf{R},0)\, E_s(\mathbf{R},t)> \propto < \delta\alpha_{is}^*(\mathbf{q},0)\, \delta\alpha_{is}(\mathbf{q},t)> e^{i\omega t} \tag{2.3}$$

If we further assume that the scatterers are spherical and isotropic

$$\delta\alpha_{is}(\mathbf{q},t) = (\mathbf{n_i}\mathbf{n_f})\, \alpha \sum_{j=1}^{N} e^{i\mathbf{q}\cdot\mathbf{r_j}(t)}. \tag{2.4}$$

Thus,

$$<E_s^*(\mathbf{R},0)\, E_s(\mathbf{R},t)> \propto \sum_{j=1}^{N} e^{i\mathbf{q}\cdot[\mathbf{r_j}(t)-\mathbf{r_j}(0)]}. \tag{2.5}$$

Assuming all the scatterers are statistically independent and that N is large enough for fluctuations in the number of particle in the scattering volume to be

insignificant, the summation can be taken outside of the ensemble average. Thus, defining $g^{(1)}(t)$ as

$$g^{(1)}(t) = \langle E_s^*(\mathbf{R},0)\, E_s(\mathbf{R},t)\rangle / \langle E_s^*(\mathbf{R},0)\, E_s(\mathbf{R},0)\rangle \tag{2.6}$$

we have

$$g^{(1)}(t) = \left\langle e^{iq[r_j(t)-r_j(0)]} \right\rangle \tag{2.7}$$

This quantity is known as the normalized self intermediate scattering function and is related to the probability distribution $G_s(\mathbf{R},t)$ for a particle to suffer a displacement $\mathbf{R}$ in the time t.

$$F_s(q,t) \equiv \left\langle e^{iq[r_j(t)-r_j(0)]} \right\rangle = \int_V d^3R\, e^{iq\cdot R} G_s(\mathbf{R},t) \tag{2.8}$$

Thus, to evaluate our correlation function we must determine $G_s(\mathbf{R},t)$ for the system. For the case of bubbles, $G_s(\mathbf{R},t)$ corresponds to the probability of finding a bubble in the neighborhood $d^3\mathbf{R}$ of point $\mathbf{R}$, at time t, given it was at the origin at time zero. The bubbles undergo Brownian motion in the solution and thus diffuse through the solution performing a random walk. Therefore, if we assume no convection $G_s(\mathbf{R},t)$ can to a very good approximation be regarded as the solution to the diffusion equation

$$\frac{\partial}{\partial t} G_s(\mathbf{R},t) = D\nabla^2 G_s(\mathbf{R},t) \tag{2.9}$$

If we perform a spatial fourier transform of Eq. 2.9 we have

$$\frac{\partial}{\partial t} F_s(q,t) = -q^2 D\, F_s(q,t) \tag{2.10}$$

The solution to this is

$$F_s(q,t) = F_s(q,0)\, e^{-Dq^2 t} \tag{2.11}$$

which gives

$$g^{(1)}(t) = e^{-Dq^2 t} \,. \tag{2.12}$$

In PCS the output of the photo-multiplier tube (PMT) is passed to an autocorrelator. Since the current of the PMT is proportional to the intensity of the electric field $i(t) \propto | E(t) |^2$, the correlator calculates the autocorrelation c(t) of i(t):

$$c(t) = \langle i(t)i(0) \rangle = B \langle | E(0) |^2 | E(t) |^2 \rangle \quad (2.13)$$

where B is a proportionality constant that depends on the PMT. The intensity autocorrelation function can be expressed in terms of the field autocorrelation function Eq. 2.12. The field E_s is a random variable with a Gaussian distribution, if this is so,

$$\langle | E(0) |^2 | E(t) |^2 \rangle = | E(0) |^4 + | \langle E_s^*(R,0) E_s(R,t) \rangle |^2 \quad (2.14)$$

or

$$c(t) \propto |g^{(1)}(0)|^2 + | g^{(1)}(t)|^2 \quad (2.15)$$

and, the autocorrelation function can be written as

$$c(t) = B [1 + e^{-2Dq^2t}] \quad (2.16)$$

In practice we find

$$c(t) = B [1 + Ae^{-2Dq^2t}] \quad (2.17)$$

where A is a constant < 1, related to the spatial coherence properties of the optical system, and depends on the number of coherence areas sampled. In practice the value of A is determined by fits to the data.

The size of the scatterers can be extracted from the diffusion function by utilizing the Stokes -Einstein relation. For rigid spherical particles in which the interface between the particle and the surrounding liquid is subjected to a no slip boundary condition we have[59]

$$D = \frac{k_B T}{6\pi\eta R} \quad (2.18)$$

For a fluid sphere, such as a bubble in a liquid, the no slip boundary condition is replaced by a condition that there can be no relative motion of the two fluids at the interface, also the tangential stresses at the interface must be equal and opposite on either side of the boundary. In this case[59]

$$D = \frac{k_B T}{4\pi\eta R} \quad (2.19)$$

For both equations k_B is Boltzmann's constant, T is the temperature, η is the viscosity of the solution, and R is the radius of the scatterers.

The corresponding spectrum $S(q,\omega)$ can be obtained by Fourier transforming the field correlation function

$$S(q,\omega) \propto \frac{1}{2\pi} \int_{-\infty}^{+\infty} e^{-i\omega t} g^{(1)}(t)\, dt \propto \frac{1}{2\pi} \int_{-\infty}^{+\infty} e^{-i\omega t}\, e^{-\Gamma t}\, dt \propto \frac{\Gamma}{\omega^2+\Gamma^2} \tag{2.20}$$

where $\Gamma=Dq^2$ is the linewidth of the spectrum.

If we have a distribution of scatterers with different Γ's then the correlation function is no longer a simple exponential. $g^{(1)}(t)$ is then made up of contributions from scatterers of many diffusion coefficients D, and can be written as

$$g^{(1)}(t) = \int e^{-\Gamma t}\, N(\Gamma)\, I(\Gamma) d\Gamma \tag{2.21}$$

where $N(\Gamma)\, d\Gamma$ is the fraction of the total intensity due to scatterers for which $Dq^2=\Gamma$.

Koppel[60] has shown that $g^{(1)}(t)$ can be expressed as a power series in terms of the cumulants of the distribution $N(\Gamma)$. Normally the first two terms of the power series are sufficient and we can write

$$c(t) = B\,[\,1 + A\,|e^{-\overline{\Gamma} t + \frac{\mu_2 t^2}{2} \cdots}|^2\,] \tag{2.22}$$

In practice, $\overline{\Gamma}$, and μ_2 are found from

$$\ln\left[\left[\frac{c(t)-B}{B}\right]^{1/2}\right] = \ln[(A)^{1/2}] - \overline{\Gamma}\, t + \frac{\mu_2}{\Gamma^2} t^2 \tag{2.23}$$

Here $\overline{\Gamma}$ is the first cumulant of $N(\Gamma)$ and μ_2 to the second.

A measure of the width of the size distribution of the scatterers can be obtained from the polydispersity index which is defined as

$$Q = \mu_2 / \overline{\Gamma}^2 \tag{2.24}$$

Generally Q is between 0 and 1. For a Gaussian distribution of bubble sizes small polydispersities of between 0 and 0.1 indicate a normalized size variance $(\sigma_R/<R>)^2$ of 0 - 20 %. for larger values of Q a conversion to normalized variance is more unreliable.

For scattering from thermodynamic fluctuations the derivation follows along similar lines, and the correlation function is again of the form of Eq. 2.17. However, the effective diffusion coefficient is now defined to be

$$D = \frac{k_B T}{6\pi\eta\xi} \tag{2.25}$$

where ξ is the correlation length of the fluctuations. Further details will be given in the section on the Ornstein-Zernike theory.

2.1.2. Mie Theory

Mie theory provides a solution for the intensity of the scattered light by means of a formal solution to Maxwell's equations. The original result was derived by Mie in 1908[63], and has been reviewed in several texts[63,64]. This is a problem of some complexity and requires the solution to be expressed as a power series. In general the approach involves transforming Maxwell's equations into a set of scalar wave equations. The solution to these equations are then expressed as three separate power series for: the field inside the scatterer, the unscattered wave and the scattered wave. The form of each series is chosen to suit the geometry of the scatterer. The coefficients for each term in these three series are then found using the boundary conditions for the particular problem. These conditions provide a set of algebraic equations that can then be solved to obtain the coefficients of the terms in the series.

For scattering from bubbles we are concerned with Mie scattering by an isotropic homogeneous sphere, of radius R and relative refractive index m. The analysis is simplest in spherical coordinates (r,θ,φ). The asymptotic form of the solution for the tangential field components of the scattered wave is given below[64].

$$E_\theta = H_\psi = -\frac{i}{kr} e^{-ikr + i\omega t} \cos\varphi \, S_2(\theta) \tag{2.26}$$

$$-E_\psi = H_\theta = -\frac{i}{kr} e^{-ikr + i\omega t} \sin\varphi \, S_1(\theta) \tag{2.27}$$

where

$$S_1(\theta) = \sum_{n=1}^{\infty} \frac{2n+1}{n(n+1)} \{a_n \pi_n(\cos\theta) + \tau_n b_n(\cos\theta)\} \tag{2.28}$$

$$S_2(\theta) = \sum_{n=1}^{\infty} \frac{2n+1}{n(n+1)} \{b_n \pi_n(\cos\theta) + \tau_n a_n(\cos\theta)\} \tag{2.29}$$

Here

$$a_n = \frac{\psi'_n(y)\psi_n(x) + m\psi_n(y)\psi'_n(x)}{\psi'_n(y)\zeta_n(x) + m\psi_n(y)\zeta'_n(x)} \tag{2.30}$$

$$b_n = \frac{m\psi'_n(y)\psi_n(x) + \psi_n(y)\psi'_n(x)}{m\psi'_n(y)\zeta_n(x) + \psi_n(y)\zeta'_n(x)} \tag{2.31}$$

and

$$\pi_n(\cos\theta) = \frac{1}{\sin\theta} P_n^1(\cos\theta) \tag{2.32}$$

$$\tau_n(\cos\theta) = \frac{d}{d\theta} P_n^1(\cos\theta) \tag{2.33}$$

$\zeta_n(z)$, $\psi_n(z)$, and $\chi_n(z)$ are the Riccati-Bessel functions, $P_n^1(\cos\theta)$ is a Legendre polynomial, and $x=2\pi R/\lambda$ and $y=mx$.

The radial component may also be calculated but tends to zero with a higher power of r^{-1}. Generally all that is computed is $i_1 = |S_1(\theta)|^2$ and $i_2 = |S_2(\theta)|^2$. The Mie coefficients described above were calculated using a computer program generously provided by Peter Barber of Clarkson Univ.

2.1.3. Light Scattering from Thermodynamic Fluctuation

In Bilgram's mesophase theory of light scattering from the crystal-melt interface[28] the strong scattering is caused by anomalously large density fluctuations in a supposed boundary layer between the crystal and melt. In this section, the theory of light scattering from fluctuations in simple fluids is reviewed briefly. In the next section the Ornstein Zernike theory of light scattering in the vicinity of the critical point[65,65] is discussed.

In contrast to scattering from microbubbles, where the scattering objects are of dimensions comparable to q^{-1} (ie 1 μm), the study of light scattering by thermal fluctuations involves fluctuations of the dielectric constant caused by the collective motion of large numbers of individual molecules. This means that we can use the laws of macroscopic continuum physics to describe their behavior.

The standard derivation[57,58,67] relates the scattered field to fluctuations in the local dielectric constant $E_s(\mathbf{q},t) \propto \delta\varepsilon(\mathbf{q},t)$. In this approach the dielectric constant ε is assumed to be in local equilibrium and is considered to be a function of the state variables density ρ and temperature T. The fluctuations in ε can then be expanded to first order in terms of the fluctuations in $\delta\rho$ and δT

$$\delta\varepsilon(\mathbf{r},t) = \left(\frac{\partial\varepsilon}{\partial\rho}\right)\delta\rho(\mathbf{r},t) + \left(\frac{\partial\varepsilon}{\partial T}\right)\delta T(\mathbf{r},t). \tag{2.34}$$

The spectral density $I(\mathbf{q},\omega)$ of the scattered light

$$I(\mathbf{q},\omega) \propto \int_{-\infty}^{\infty} dt\, e^{\omega t} \langle \delta\varepsilon(\mathbf{q},0)\delta\varepsilon(\mathbf{q},t)\rangle \tag{2.35}$$

$$\propto S_{\varepsilon\varepsilon}(\mathbf{q},\omega)$$

is now expressed as

$$I(\mathbf{q},\omega) \propto \left(\frac{\partial\varepsilon}{\partial\rho}\right)^2 S_{\rho\rho}(\mathbf{q},\omega) + \left(\frac{\partial\varepsilon}{\partial\rho}\right)\left(\frac{\partial\varepsilon}{\partial T}\right)\left[S_{\rho T}(\mathbf{q},\omega) + S_{T\rho}(\mathbf{q},\omega)\right] + \left(\frac{\partial\varepsilon}{\partial T}\right)^2 S_{TT}(\mathbf{q},\omega) \tag{2.36}$$

where the $S_{AB}(q,\omega)$ refers to the spectral density of the correlation function $<\delta A^*(q,0),\delta B(q,t)>$. For most systems it is found that $\frac{\partial \varepsilon}{\partial T} << \frac{\partial \varepsilon}{\partial \rho}$. Therefore,

$$I(q,\omega) \propto S_{\rho\rho}(q,\omega) \tag{2.37}$$

Consequently, the spectral density of the scattered light can be found if the spectral density of the autocorrelation function of the density fluctuations is known. The standard approach for deriving $S_{\rho\rho}(q,\omega)$ in a fluid uses the macroscopic equations of fluid mechanics. This derivation leads to the well known Rayleigh-Brillouin spectrum[68]. $S_{\rho\rho}(q,\omega)$ is essentially found to be comprised of three peaks

$$S_{\rho\rho}(q,\omega) \propto (\gamma-1)\frac{D_T q^2}{\omega^2 + [D_T q^2]} + \frac{\Gamma_a q^2}{[\omega-\omega(q)]^2 + [\Gamma_a q^2]^2} + \frac{\Gamma_a q^2}{[\omega+\omega(q)]^2 + [\Gamma_a q^2]^2} \; . \tag{2.38}$$

The first term is the quasielastic Rayleigh line and corresponds to the relaxation by thermal diffusion of the non-propagating density fluctuations in the fluid (D_T is a thermal diffusivity). The other two terms form the Brillouin doublet. These Brillouin components are caused by propagating density fluctuations (sound waves) of angular frequency $\omega(q)$. Γ_a is the acoustic attenuation coefficient, and $\gamma = c_p/c_v$ is the ratio of the constant pressure to constant volume specific heats. A typical Rayleigh-Brillouin spectrum is illustrated in Fig 2.2.

If we integrate Eq. 2.38 with respect to ω the total scattered intensity can be written as $I = I_R + 2I_B$ where I_R and I_B are the contributions from the Rayleigh and Brillouin peaks respectively. The ratio $I_R/2I_B$ is known as the Landau-Placzek ratio and is equal to $(\gamma - 1)$.[69,70]

The integrated (with respect to ω) intensity I(q) is proportional to S(q), the structure factor. S(q) is given by the mean square fluctuation of the q^{th} fourier component of the density fluctuations:

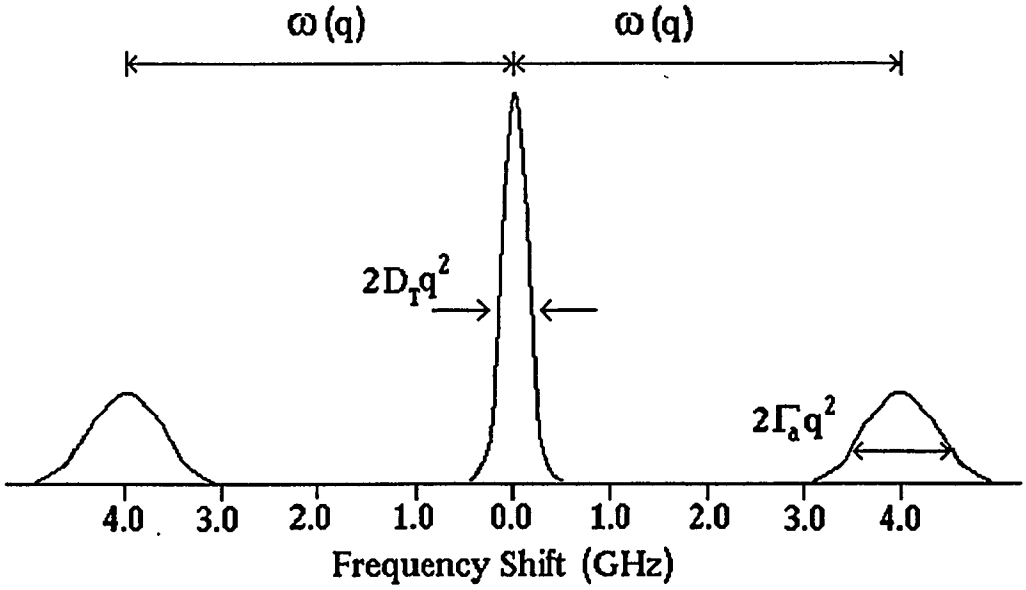

Fig 2.2: A sketch of a typical Rayleigh Brillouin spectrum.

$$S(q) = < |\delta\rho(q)|^2 > . \tag{2.39}$$

In an equilibrium fluid away from the critical region, the density varies significantly only over regions of the size of the intermolecular interactions, thus in calculating the Fourier components of $\delta\rho$ we can ignore the q dependence. This case, which always applies in the $q \to 0$ limit, gives

$$\lim_{q\to 0} \delta\rho(\mathbf{q}) = \lim_{q\to 0} \int_V d^3r\, e^{i\mathbf{q}.\mathbf{r}}\, \delta\rho(\mathbf{r}) = \int_V d^3r\, \delta\rho(\mathbf{r}) = \delta N. \tag{2.40}$$

Thus, Eq. 2.40 relates the integrated scattered intensity to the fluctuations in the number of particles in the scattering volume δN. $< \delta N^2 >$ can be calculated from statistical fluctuation theory (see appendix 10.A in Ref. 58) and is related to the isothermal compressibility χ_T.

$$\lim_{q\to 0} S(q) = < N^2 > = V\rho^2 k_B T \chi_T \tag{2.41}$$

In this approximation the scattering is independent of angle.

In the mesophase model[28] the intense scattering at the interface is ascribed to a boundary layer between the crystal and melt with a large χ_T (in the ice water system

this is calculated to be 700 times the usual value for water at 0°C). The scattering is found to arise from the central peak in the spectrum in Eq. 2.38. D_T is interpreted as an effective thermal diffusion constant that describes the transport of heat involving fluctuations of order and disorder in the layer. It is assumed[28] that D_T can be related to the coherence length of the fluctuations ξ by a Stokes Einstein relation of the form

$$D_T = \frac{k_B T}{6\pi\eta\xi} \tag{2.42}$$

The value of ξ so extracted from the dynamic light scattering measurements is in the range 20 − 80 nm for the ice water system[18,19,28,32] and in the range 0.1 - 1.0 μm for salol[29] and cyclohexane[33]. These values of ξ are comparable to q^{-1}. Thus, the assumption of q independence in Eq 2.40 is no longer valid, and within the framework of this model one would expect the scattered intensity to vary with angle. In order to predict S(q) one must include the q dependence in the calculation of $\delta\rho(q)$. The problem of calculating S(q) for systems with large density fluctuations arises in the study of simple fluids and binary systems in the vicinity of the critical point. In the next section the Ornstein Zernike theory for scattering in the critical region is reviewed.

2.1.4. The Ornstein-Zernike Theory

Ornstein-Zernike theory[65,66,71,72] describes the scattering of light by either a simple fluid or a binary mixture in the vicinity of the critical point. Near this phase transition fluids that were previously clear strongly scatter light and appear milky. This strong scattering is due to a large isothermal compressibility, which is associated with the long range correlations in the density fluctuations that occur in this region. This phenomenon is known as critical opalescence.

For systems where the range of the density fluctuations are of order q^{-1} evaluation of Eq 2.40 for S(q) requires including the q dependence in the Fourier transformation. The integral can now be written as

$$S(q) = \langle |\delta\rho(q)|^2 \rangle = \iint dr dr' \, e^{iq.(r-r')} \langle \rho(r)\rho(r') \rangle \tag{2.43}$$

$$= \iint dr dr' \, e^{iq.(r-r')} \, G(r,r') \tag{2.44}$$

$$= V \int e^{iq.R} \, G(R) \tag{2.45}$$

In the last step the variable $R = r - r'$ has been introduced. Thus, the structure factor is related to the Fourier transform of the density density correlation function G(R). Here it is also assumed that as the system is spatially invariant, and G(r,r') will only be a function of R.

It can be seen from Eq 2.43 that if there are no particle correlations the cross terms would cancel and $S^0(q) = \langle N \rangle$. Therefore, the deviation of $S(q)/S^0(q)$ from 1 reflect the spatial correlation in the system.

$$\frac{S(q)}{S^0(q)} = \frac{1}{\rho} \int e^{iq.R} \, G(R) \tag{2.46}$$

The Ornstein and Zernike approach to the problem involves first separating G(R) into a term due to self correlations and a term due to correlations between different particles $\Gamma(R)$.

$$G(R) = \rho\delta(R) + \rho^2\Gamma(R) \tag{2.47}$$

giving

$$\frac{S(q)}{S^0(q)} = 1 + \rho \int e^{iq.R} \, \Gamma(R) \tag{2.48}$$

Ornstein and Zernike then introduced the concept that $\Gamma(R)$ is related to a short range interaction between pairs of atoms C(R). $\Gamma(R)$ is then the sum of a direct correlation and an indirect correlation between all other points.

$$\Gamma(R) = C(R) + \rho \int C(R')\Gamma(R-R') \, dR' \tag{2.49}$$

Eq. 2.49 is illustrated schematically in Fig. 2.3. Fourier transforming Eq. 2.49 and inserting the result into Eq. 2.48 leads to

$$\frac{S(q)}{S^0(q)} = \frac{1}{1-\rho C(q)} \tag{2.50}$$

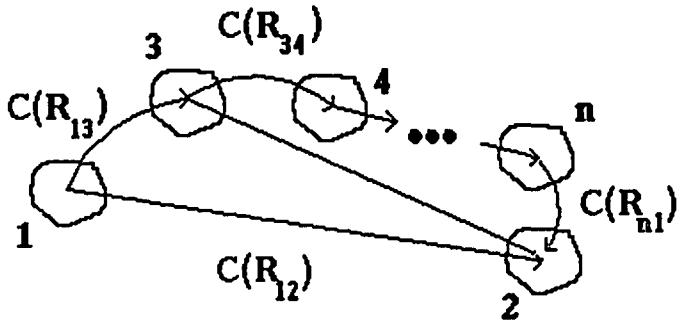

$$\Gamma(R_{12}) = C(R_{12}) + \int C(R_{13})\Gamma(R_{23})dR_3$$

Fig 2.3: Sketch that illustrates the two terms that make up the total correlation function $\Gamma(\mathbf{R})$. The first term in which particles 1 and 2 are correlated directly through $C(\mathbf{R})$. The second in which the correlation comes about through the aggregate correlation of the other atoms in the fluid.

Examining the properties of $C(\mathbf{q})$, we note that at high temperature the system should resemble a normal fluid, so that $\frac{S(q)}{S^0(q)} \to 1$ and $C(\mathbf{q})$ will be 0. However, as $T \to T_c$, we expect $\lim_{q\to 0} \frac{S(q)}{S^0(q)} \to \infty$ and so $\lim_{q\to 0} C(q) \to \rho^{-1}$. This implies that $C(\mathbf{R})$ is a short ranged well behaved function of $\mathbf{R}$, and integrals of the form $\int_0^\infty d^3R\, R^l\, C(\mathbf{R})$ are finite. This permits $C(\mathbf{q})$ to be expanded in powers of q. Ornstein and Zernike also assumed $C(\mathbf{q})$ to be a slowly varying function of q and thus the series can be approximated by the first two terms. Therefore,

$$C(\mathbf{q}) = C_0 - C_2\, q^2 \qquad (2.51)$$

where

$$C_0 = 4\pi \int_0^\infty dR\, R^2\, C(R) \tag{2.52}$$

$$C_2 = \frac{2\pi}{3} \int_0^\infty dR\, R^4\, C(R)\,. \tag{2.53}$$

If Eq. 2.51 is substituted back into Eq. 2.50 we have

$$\frac{S^0(q)}{S(q)} = R_0^2[\, q_0^2 + q^2] \tag{2.54}$$

with

$$R_0^2 \equiv \rho C_2 \qquad q_0^2 \equiv \frac{1-\rho C_0}{R_0^2} \tag{2.55}$$

As $q \to 0$ we see from Eq 2.54 that

$$\lim_{q\to 0} \frac{S^0(q)}{S(q)} = R_0^2 q_0^2 = \beta(\rho\chi_T)^{-1} \tag{2.56}$$

Where $\beta = (k_B T)^{-1}$ and the last equation again follows from the application of statistical fluctuation theory (see appendix 10.A of ref 58). Thus, defining $q_0^{-1} = \xi$ and inserting Eq 2.56 into Eq 2.54

$$\frac{S(q)}{S^0(q)} = \beta^{-1}\rho\chi_T \left[\frac{1}{1 + (q\xi)^2} \right] \tag{2.57}$$

This result corresponds to the Ornstein-Zernike spatial correlation function

$$G(R) \propto \frac{1}{R_0^2} \frac{e^{-\xi R}}{R} \tag{2.58}$$

Eq. 2.57 is the Ornstein-Zernike form for the scattered intensity, and was used by Bilgram to model the angular dependence of the light scattered from the interface.

2.2. The Theory of Gas Bubbles in Liquids

2.2.1. The Theory of Bubble Formation

We shall start by introducing the concept of a critical radius R_c. Once a gas bubble is created in a solution, it will either grow or decay depending on whether it is larger or smaller than the critical radius which is that radius at which the bubble is in (unstable) equilibrium with the liquid that surrounds it.

To derive the critical radius we consider a closed system at a uniform constant temperature and constant volume. Following the treatment of Ward *et. al.* [73], the free energy F is a function of: the volume V_l and entropy S_l of the liquid, the volume V_g and entropy S_g of the bubble, the number of gas molecules in the bubble N_g and in the liquid N_l, and the area A of the surface of the bubble. The differential of the free energy is given by

$$dF = -SdT - P_l dV_l - P_g dV_g + \sigma dA + \mu_l dN_l + \mu_g dN_g \qquad (2.59)$$

Here $S = S_l + S_g$,, σ is the surface tension and μ_l and μ_g are the chemical potentials of the gas molecules in the bubble and the liquid. As the system has a constant total volume and number of gas molecules, then

$$dV_l = - dV_g \qquad (2.60)$$

$$dN_l = - dN_g \qquad (2.61)$$

For the system to be at equilibrium $dF=0$. If the system is isothermal ($dT=0$) and in chemical equilibrium ($\mu_l = \mu_g$), then this condition applied to Eq 2.59 along with Eq. 2.60 and Eq. 2.61, gives

$$P_g - P_l = \sigma \frac{dA}{dV_g} \qquad (2.62)$$

Therefore, if we assume that the bubble is spherical we find the critical radius R_c to be

$$R_c = \frac{2\sigma}{P_g - P_l} \qquad (2.63)$$

The required free energy to create a bubble is[73]

$$\Delta F_c = (P_g - P_l)V_g + \sigma A \qquad (2.64)$$

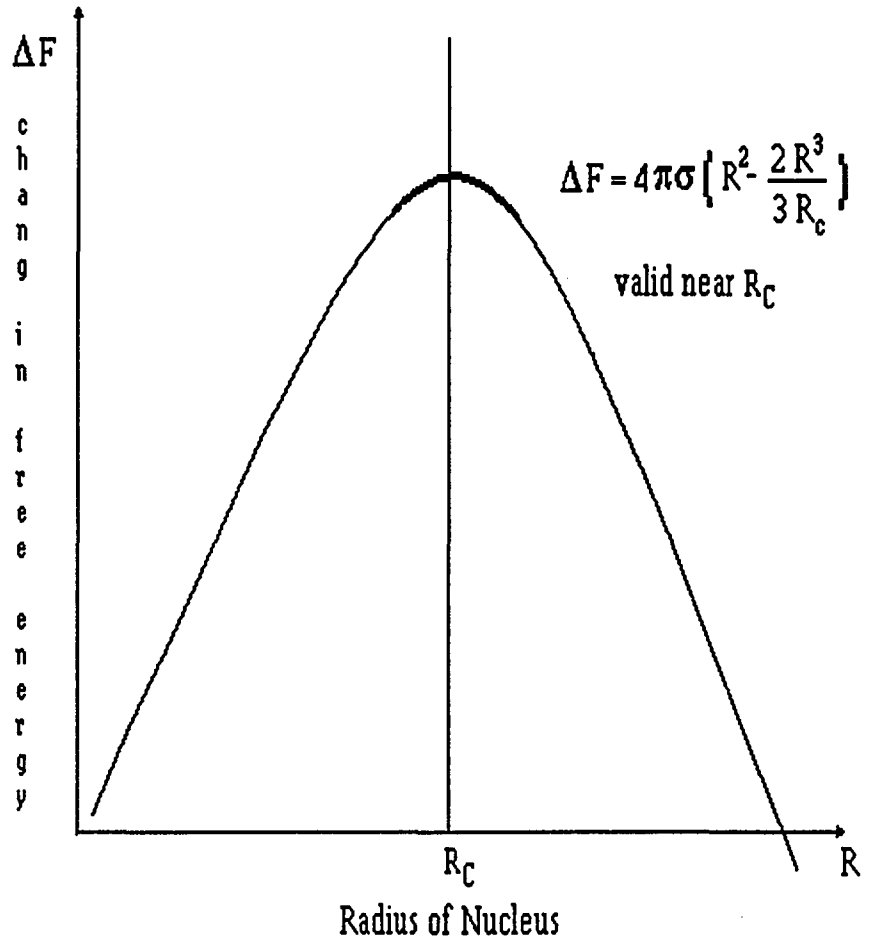

Fig 2.4: Cost in free energy of creating a bubble of size r vs r. The maximum of the curve gives the critical radius.

Inserting the value for R_c from Eq. 2.63 into Eq. 2.64 we find that the necessary free energy for the formation of a bubble radius R_c is

$$\Delta F_c = \frac{4\pi}{3}\sigma R_c^2 \tag{2.65}$$

We also note, by expanding ΔF_c around R_c, that the free energy is of the form

$$\Delta F_c = 4\pi\sigma(R^2 - \frac{2R^3}{3R_c}) \tag{2.66}$$

This relation is shown in Fig 2.4. From this we see that this equilibrium point is an unstable one.

Next, we consider the bubble nucleation problem. First we shall consider homogeneous nucleation of a bubble, that is nucleation within the bulk of the liquid. Then we shall consider heterogeneous nucleation which is nucleation aided by a surface or impurity of some sort. From thermodynamics we can predict that the rate at which fluctuations of the gas concentration in the liquid will spontaneously produce a nucleus of radius R_c is of the form

$$J = A\, e^{-\Delta F_c / k_B T} \tag{2.67}$$

The form of the pre-exponential factor A is a matter of some controversy. We shall use a form proposed by Hirth *et. al.*[74]

$$A = (\alpha\, C_l V_v / V_g) \sqrt{\frac{2\sigma}{pM}} \tag{2.68}$$

where α is called the accommodation coefficient (sticking fraction), z is the compressibility factor (= 1 for ideal gas) and M is the mass of the gas molecules. C_l is the molecular concentration in the liquid, V_v is the volume of the bubble, and $V_g = k_B T z / P_g$ is the molecular volume in the nucleated bubble. It has been conjectured by Wilcox and Kuo that C_l should be the gas concentration in the liquid. From Eq 2.65 and Eq. 2.63 we have

$$\Delta F_c = \frac{16\pi\sigma^3}{3(P_g - P_l)^2} \tag{2.69}$$

and thus combining Eq.2.67, Eq.2.68 and Eq.2.69, the homogeneous nucleation rate is

$$J = (\alpha C_l V_v / V_g) \sqrt{\frac{2\sigma}{pM}}\, e^{\frac{-16\pi\sigma^3}{3k_B T(P_g - P_l)^2}} \tag{2.70}$$

In the case of heterogeneous nucleation the bubbles are nucleated at a surface (see Fig 2.5). For a plane surface the differential free energy is now

$$dF = -SdT - P_l dV_l - P_g dV_g + \sigma_{lg} dA_{lg} + (\sigma_{sg} - \sigma_{ls}) dA + \mu_l dN_l + \mu_g dN_g \tag{2.71}$$

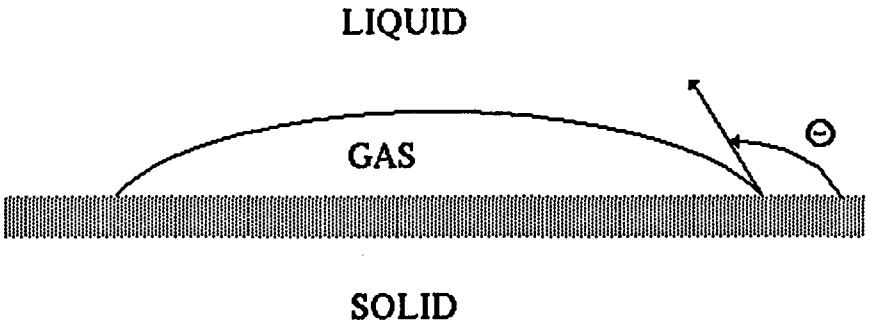

Fig 2.5: Heterogeneous nucleation at a surface

Where σ_{lg} is the liquid-gas surface energy, σ_{sg} is the solid-gas surface energy, and σ_{ls} is the solid-liquid surface energy. In this case it can be shown that the critical free energy changes to[2]

$$\Delta F_c = \frac{\phi 16\pi\sigma_{lg}^3}{3(P_g - P_l)^2} \qquad (2.72)$$

where $\phi = (2 - \cos\theta)(1 + \cos\theta)^2/4$. θ is the contact angle between the liquid and solid surface $\cos\theta = (\sigma_{sg} - \sigma_{ls}) / \sigma_{lg}$: When $(\sigma_{sg} - \sigma_{ls}) > \sigma_{lg}$ then $\theta = 0$. This case corresponds to perfect wetting of the solid surface by the liquid, and nucleation is unaffected. When $(\sigma_{sg} - \sigma_{ls}) \leq \sigma_{lg}$ then $\theta = 180°$ and the liquid doesn't wet the solid at all. For this case nucleation would be greatly enhanced. However, this case is unlikely as usually $\sigma_{sg} \gg \sigma_{ls}$ and $\sigma_{sg} > \sigma_{lg}$. For example for an air bubble at the ice-water interface we have $\sigma_{sg} = 109$ dyn/cm $\sigma_{ls} = 33$ dyn/cm and $\sigma_{lg} = 75.6$ dyn/cm, which corresponds to the case of perfect wetting, (the values of the surface energies have been taken from Ketchem and Hobbs[75]). As bubbles do generally nucleate at saturation considerably less than that predicted by homogeneous nucleation theory,[14,15] the surface roughness must play an important role in lowering the activation energy for nucleation. Also, large amounts of gas dissolved in the liquid may alter the surface energies[2]. A further possibility is that submicroscopic nuclei may already be trapped in

the interstices of the particles that constitute the surface, so that all that is required of the local environment is that it be favorable for bubble growth.

Eq. 2.70 can be used to predict the gas pressure necessary to nucleate an observable quantity of bubbles in the homogenous case. If we assume a minimum necessary nucleation rate J_{min} of 1 bubble /cm^{3}sec P_g, must satisfy

$$P_g \geq P_l + (16\pi\sigma^3\phi)^{1/2} \left\{ 3k_BT \ln \left[(\alpha C_l V_v P_g / z k_B T J_{min}) \sqrt{\frac{2\sigma}{pM}} \right] \right\}^{-1/2} \quad (2.73)$$

Eq 2.73 can be iterativly solved for P_g. This has been done by Wilcox and Kuo[2] who found for air in naphthalene ($P_g - P_l$) = 380 atm, and for air in water ($P_g - P_l$) = 1720 atm. These pressures correspond to critical radii of R_c = 16.8Å and R_c = 8.6Å respectively.

2.2.2. Bubble Growth and Stabilization

Epstein and Plesset[76] have studied the stability of gas bubbles once they are formed. Their approach is based on the assumption that the bubble will change its size as gas moves across the boundary by diffusion. The calculation is done in the approximation that the bubble is stationary. This they claim is a reasonable approach as bubbles of radius ~ 1 μm have a terminal velocity of ~ 1 μm/sec. The gas concentration in the liquid around the bubble must satisfy the diffusion equation.

$$\frac{\partial C}{\partial t} = D \frac{\partial^2 C}{\partial x^2} \quad (2.74)$$

D is the coefficient of diffusivity of the gas in the liquid. The boundary conditions are

$$C(r,0) = C_i \, , \, r > R \qquad \lim_{t \to \infty} C(r,t) = C_i, \, t > 0$$
$$C(R,t) = C_s, \, t > 0 \quad (2.75)$$

where C_s is the saturation concentration of the liquid, C_i is the average gas concentration in the liquid, and R is the radius of the bubble. After an appropriate

change of variables the diffusion Eq. 2.74 can be solved and the concentration profile of the gas in the liquid around the bubble can be ascertained. It is then straightforward to relate the concentration gradient of the gas in the liquid at the boundary, to the rate of change of mass and thus the radius of the bubble. They find

$$\frac{dR}{dt} = \frac{D\delta}{\rho}\left\{\frac{1}{R} + \frac{1}{(\pi\Delta t)^{1/2}}\right\} \tag{2.76}$$

where $\delta = (C_i - C_s)$, and ρ is the density of the liquid. Eq. 2.76 can then be readily solved. If we define $f = C_i/C_s$, for undersaturation ($0 \leq f < 1$) the bubble will shrink, while for supersaturation ($f > 1$) the bubble will grow.

For the undersaturated case the approximate solution to Eq. 2.76 is

$$\left[\frac{R}{R_i}\right]^2 = 1 - \left[\frac{2\alpha}{R_i^2}\right] t \tag{2.77}$$

Where R_0 is the initial bubble radius. Using Eq. 2.77 we can estimate the time for a bubble to disappear. Numerical results for the approximation given by Eq. 2.77, and the exact solution of Eq. 2.76 are given in table 2.1, for 1 μm air bubbles in water. For growth in an oversaturated solution

$$\left[\frac{R}{R_i}\right]^2 = 1 + \left[\frac{2\alpha}{R_i^2}\right] t \tag{2.78}$$

In table 2.1 we also give the time for 1 μm air bubbles in water to grow to ten times their original size.

It can be seen from table 2.1 that once bubbles drift out of a supersaturated region, their lifetime predicted by Eq. 2.76 is short. However, there are several models for the stabilization of microbubbles in liquids. These models which have been reviewed by Crum,[77] include the "rigid organic skin model",[78] the "ionic skin model"[79] the "film of surface-active substance model"[80] and the "crevice model".[81]

In the rigid skin model Fox and Herfeld[78] note that organic compounds are often surface active, and they propose that when bubbles are formed in these compounds, a rigid skin may be formed about the surface of the bubble which prevents

Time for disappearance			Time to grow to 10 R_0		
f	T (sec)	T_A (sec)	f	T (sec)	T_A (sec)
0.00	1.05	1.25	1.25	466	496
0.25	1.44	1.67	1.50	228	248
0.50	2.11	2.50	1.75	149	165
0.75	4.58	5.00	2.00	110	124
1.00	∞	∞	5.00	24.6	30.9

Table 2.1: Times for disappearance and growth of 1μm bubbles in undersaturated and supersaturated solutions. T corresponds to the approximate solutions of Eq. 2.76 given by Eq. 2.77 and Eq. 2.78. T_A corresponds to the exact solution of Eq. 2.76. Values taken from Ref. 74

it from dissolving. The origin of the "ionic skin model"[79] lies in the observation that air bubbles in water possess some electrical charge. It thus seems possible that the repulsion of like charges on the surface could stabilize the bubble. The "film of surface-active substance model"[80] applies to the stabilization of bubbles by components in the liquid that are surface active. For example detergent or soap molecules have oxygen rich groups on one end and long chain hydrocarbon tails on the other end. The polar head group will attach to water, and the tail will extend into the air. Thus, a thin film of the molecules can envelope the bubble and will have a certain elasticity that will stabilize it. In the crevice model[81] gas is trapped in conical crevices in solid inhomogeneities in the liquid. This model has been successful in explaining many aspects of nucleation and boiling.[77]

2.2.3. Trapping of Bubbles in Crystallizing Solids

As we have seen in the introduction (Sec. 1.1), it is quite common for bubbles to be trapped in a crystal. Chernov and Temkin[82] have reviewed the phenomenon of trapping of inclusions in crystal growth, and they discussed the conditions for trapping in terms of a disjoining pressure. The major experimental fact is that foreign particles in a crystalizing solution will be pushed along with the interface as long as the growth velocity does not exceed a critical value v_c. This velocity decreases with increasing particle size. Disjoining pressure is the term that Chernov and Temkin give for the force that repulses the particle. The essential origin of this disjoining pressure is that the effective free energy of the system, consisting of the particle, the crystal, and the film of liquid that joins them, changes as the particle approaches the interface. The effective free energy of the complex particle-film-solid interface α_{eff}, changes from $\alpha + \alpha_{pl}$ to α_{ps} as the particle approach the interface. Here α, α_{pl} and α_{ps} are the specific free energies of the solid-liquid, particle-liquid and particle-solid interfaces. If $\alpha_{ps} > \alpha + \alpha_{pl}$, α_{eff} must decrease with increasing film thickness. Thus, the disjoining pressure is repulsive. In the article[82] they find that the critical velocity scales as $R^{-4/3}$ for small particles ($\lesssim 100\ \mu m$) and scales as R^{-1} for large particles. They plot these relationships against several sets of experimental data.

2.3. Theories of Anomalous Light Scattering at the Crystal Melt Interface

2.3.1. The Microbubble Model

Cummins *et. al.*[38] proposed the microbubble model in 1986 after performing a preliminary study of the dependence of the scattered intensity $I(\theta)$ on the scattering angle θ in salol. This study showed that $I(\theta)$ decreases too rapidly with increasing θ to be described by an Ornstein-Zernike form characteristic of thermodynamic density (or entropy) fluctuations, but could be fit with a Mie scattering function for spheres of the size indicated by the effective diffusion constant deduced from the correlation function. [In contrast to this result, Steininger and Bilgram[33] measured the angular dependence

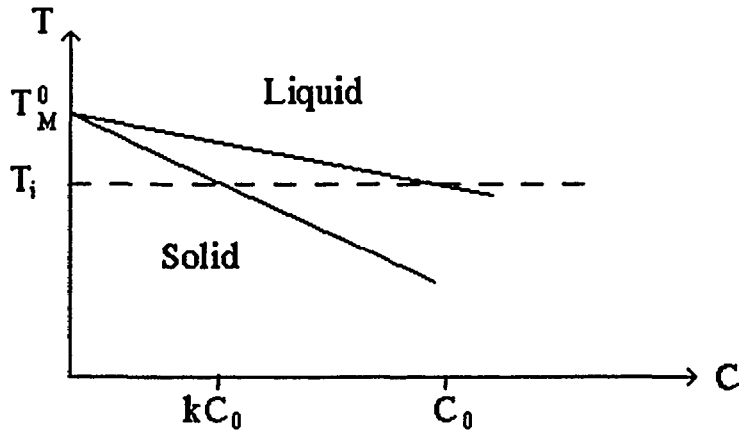

Fig 2.6: Phase diagram of a two component system. At a given temperature T, the equilibrium concentration C of the (gaseous) solute in the liquid are given by the intersection of a horizontal line at T with the upper (liquidus) and lower solidus lines respectively

of the scattered intensity for cyclohexane and found that their data fit the Ornstein-Zernike form but not the Mie form!]

The microbubble model[38] is based on the assumed existence of dissolved gaseous impurities in the melt. If the segregation coefficient k is sufficiently small, the resulting buildup of segregated dissolved gas in the melt ahead of the advancing interface can reach a level sufficient to allow heterogeneous bubble nucleation to occur. To understand this model in more detail we refer to Fig 2.6 which is the standard two component phase diagram. From this figure we see that if the liquid contains a background concentration of impurity C_0, it can coexist with a solid at concentration kC_0. Thus, when solidification begins the initial concentration profile is a step function from kC_0 in the solid to C_0 in the liquid. This profile is shown in fig 2.7(a), where $z=0$ is the instantaneous position of the interface. We assume that $k < 1$ which is usually, though not always, true.

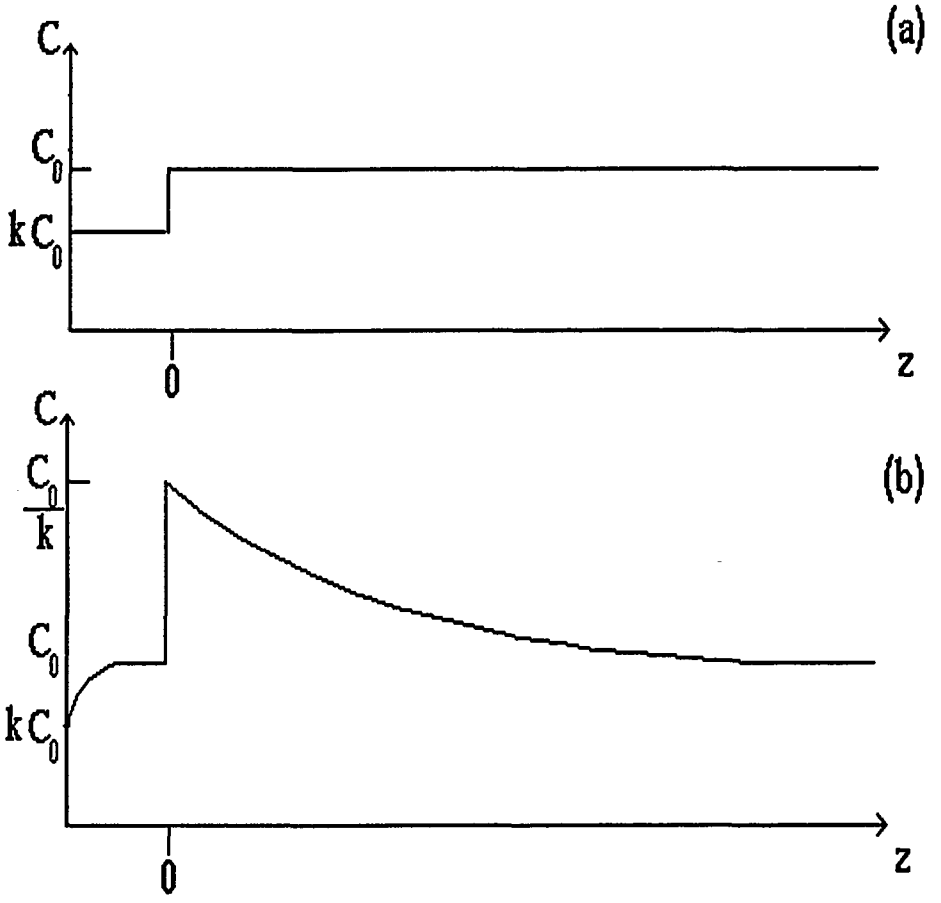

Fig 2.7: (a) Concentration profile of the solute plotted as a function of position relative to the interface (z=0) at the beginning of solidification. (b) concentration profile of solute after steady state has been reached. The solute concentration ahead of the interface has increased from its initial value of kC_0 as the interface concentration builds up due to solute rejection. At steady state, the crystal grows with solute concentration C_0, equal to the original concentration in the liquid, while the concentration C_i in the fluid adjacent to the surface is C_0/k.

Since the excess impurity is rejected by the solidifying crystal, the concentration will build up ahead of the advancing solidification front. In the frame of reference

moving with the interface, the impurity concentration C(z) must satisfy both the diffusion equation in the bulk

$$D\left(\frac{\partial^2 C}{\partial z^2}\right) + v_g\left(\frac{\partial C}{\partial z}\right) = \left(\frac{\partial C}{\partial t}\right) \tag{2.79}$$

and the continuity equation at the interface

$$C_i(k-1)v_g = D\left(\frac{\partial C}{\partial z}\right)_{z=0} + \left(\frac{\partial C}{\partial t}\right)_{z=0} \tag{2.80}$$

where z is the distance into the fluid measured from the solidification front, v_g is the growth velocity, $C_i = C(z)_{z=0}$ is the concentration in the fluid in contact with the solidification front, and D is the impurity diffusion constant in the fluid. At steady state, Eqs. 2.79 and 2.80 are solved by[38]

$$C(z) = C_o\left[1 + \frac{1-k}{k} e^{-v_g z/D}\right] \tag{2.81}$$

so that $C(z)_{z=0} = C_o/k$ which can be much larger than C_o if $k \ll 1$. The steady-state solution of Eq. 2.81 is shown in Fig. 2.7(b). Note that the thickness of the high-concentration boundary layer is given by Eq. 2.81 as

$$d = \frac{D}{v_g} \tag{2.82}$$

i.e., the thickness of the boundary layer increases as the inverse of the growth speed.

Next, consider a bubble of gas of radius R. If surface tension is neglected, then a bubble of <u>any</u> radius could exist in equilibrium with the fluid if the concentration C were exactly the saturation concentration C_s. When surface tension is included, however, bubbles can only exist in equilibrium if the liquid is supersaturated, i.e. if $f = C/C_s > 1$. If the fluid pressure is P_l and the surface tension is σ, then the effective pressure inside the bubble will be $P_g = P_l + 2\sigma/R$ (from Eq. 2.63), and bubbles can exist in (unstable) equilibrium only if $f = P_g/P_l = 1 + (2\sigma/Rp)$, where Henry's Law has been assumed to apply (the equilibrium pressure of the gas in the bubble is linearly related to its concentration in the liquid[2]). Thus, we have

$$R_c = \frac{2\sigma}{[P_l(f-1)]} \tag{2.83}$$

where P_l is assumed to be the vapor pressure of gas in equilibrium with liquid having dissolved gas concentration C_s. Bubbles with $R < R_c$ will collapse, while those with $R > R_c$ will grow.

As solidification proceeds, the solute concentration at the interface C_i will gradually increase from the initial C_o towards C_o/k. (It may never reach the steady state value because of bubble nucleation or convection.) Once it passes the saturation value C_s, however, the system may become unstable against the formation of bubbles. Initially, the critical radius R_c given by Eq.2.83 will be very large. As the concentration continues to increase, however, R_c may eventually decrease to a value small enough to allow bubbles to nucleate as shall be discussed in Sec. 5.2.

2.3.2. The Mesophase Model

The only model, other than the microbubble model, currently claimed to explain the diffusive scattering is the mesophase model[28]. In his 1987 review[30] Bilgram formulated the theory of the formation of the mesophase boundary layer in terms of a wetting transition. He suggested that the solid-liquid interface is not a two-dimensional plane, but possesses a finite thickness which scales with the correlation length ξ of density fluctuations in the layer. It was proposed that at equilibrium this phase is restricted to a microscopically thin layer by its imperfect wetting properties. (Several theoretical and computer simulation studies have indeed indicated that a thin preordered phase such as this exists, but extending only a few atomic layers into the fluid.[83]) Upon initiation of growth the system passes into a non-equilibrium state, where the liquid phase is supercooled and in contact with the crystal. After a critical growth rate has been attained, at a low enough thermal gradient, a wetting transition is assumed to take place. The mesophase then perfectly wets the interface, which enables it to grow from microscopic to macroscopic dimensions. From the hysteretic behavior of the scattering it was concluded that the transition is first order.

This interfacial boundary layer in the ice-water system is assumed to possesses an isothermal compressibility χ_T some 700 time greater than ordinary water. (a value determined by forcing the scattered intensity data to fit the mesophase theory.) Thus, the large thermodynamic density fluctuations cause the light to be scattered strongly (see Eq. 2.41) while the corresponding decay in the thermal diffusion constant causes the Rayleigh line to be very narrow compared to normal water.

3. MATERIALS AND METHODS

3.1. Salol

3.1.1. Description

Salol (phenyl salicylate $C_{13}H_{10}O_3$) when grown as a single crystal is a clear highly anisotropic material, with a convenient melting temperature of 41°C. Its structure is shown below.

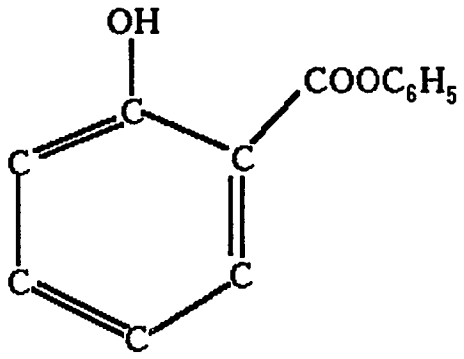

Fig 3.1: Chemical structure of salol

Salol crystallizes with an orthorombic unit cell. The unit cell dimensions at room temperature are[84]

$a = 11.25$ Å $b=25.50$ Å and $c=8.10$ Å

It is a highly birefringent crystal; the refractive indices along the three crystalline axes are

$n_a=1.66 \pm 0.02$ $n_b=1.83 \pm 0.03$ $n_c=1.55 \pm 0.02$

These values were measured by M. Awal by a method described in his Ph. D. thesis.[85] The refractive index of the melt is $n_m=1.598 \pm 0.008$ which was measured by O. Mesquita and described in his Ph. D. thesis.[86] The viscosity at T=41°C is η = 0.08 Poise. Salol is a highly faceting material with slow growth kinetics. At low growth speeds it crystallizes by a screw dislocation mechanism.

3.1.2. Sample Preparation

The salol used was purchased from Aldrich Chemical Company (99 % purity). As salol possesses a highly anisotropic crystalline structure, and displays extremely slow growth kinetics it was necessary to grow our salol crystals from seed crystals. The seed crystals used in these experiments were made by O. Mesquita, by a process described in his Ph. D. thesis.[86] The seed crystals were small single crystal cylinders oriented with the axis of interest (b in our case) down the axis of the cylinder. These seeds were then placed in the growth tube. Our growth tube consisted of thick wall Pyrex tubing, roughly 50 cm long, inside diameter 16mm, outside diameter 23mm. The tubes were fitted with high vacuum stopcocks, which allowed the sample to be kept under vacuum after filling. The growth tubes were meticulously cleaned before the seed was introduced. After introduction of the seed through the bottom of the growth tube, the tube was flame sealed closed. Triply distilled salol was then distilled into the growth tube. The filled tube was placed in the main crystal growth apparatus where most of the experiments were performed. This apparatus is described in a Sec. 3.3.2. The distilled salol was then melted back to the seed, and the crystal was grown slowly from the seed at a growth velocity of 0.0423 μm/s for this first pass. At the end of the pass we removed the last 2cm of crystal, where most of the impurity had been collected, and replaced it with freshly distilled material. Usually, several more passes were performed at faster velocities, each time replacing the last 2 cm. The sample was then ready for the light scattering experiment. Some samples were prepared by bubbling either helium or nitrogen through the sample.

3.2. Succinonitrile

3.2.1. Description

Succinonitrile ($C_4H_4N_2$) is a clear, relatively isotropic plastic organic crystal. It has a melting temperature of 58 °C. It's chemical structure is shown below.It has a cubic crystal structure. The refractive index of its melt is $n_m=1.417$,[47] the viscosity at T=58 °C. is η = 0.026 Poise, and the molecular weight is 80.09 amu. Succinonitrile grows with an atomically rough interface and is characterized by rapid growth kinetics.

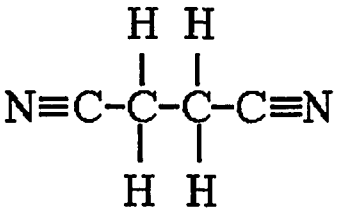

Fig 3.2: Chemical structure of succinonitrile.

3.2.2. Sample Preparation

The succinonitrile used was purchased from Fluka chemicals (99% purity). For succinonitrile the sample preparation was somewhat simpler than that for salol. The same design sample cells were used. However, as succinonitrile grows with an atomically rough interface it was not necessary to start the crystal growth with a seed crystal. It was possible to fill the cleaned sample cells with the succinonitrile and, provided the sample was clean enough, after melting and slowly recrystallizing, a suitable interface was formed when the sample was placed in the thermostat and a temperature gradient established. Several different grades of succinonitrile were used. If one was very careful with the distillation, it was found that triply distilled material was sufficiently degassed to produce virtually no scattering. Therefore, for the onset measurements singly distilled succinonitrile was used. This produced the best

compromise between dust contamination and sufficient gas concentration. For the angular intensity measurements samples with a very high gas concentration were needed because it was found that at higher gas concentrations the size of the bubbles produced was smaller. To adequately differentiate between Mie and Ornstein-Zernike scattering, bubbles of radius $0.2 < R < 0.6\ \mu m$ were required. Thus, for the angular intensity measurements, the sample tubes were loaded with undistilled succinonitrile, and placed in the main apparatus in a zone refining configuration. The samples were then put under vacuum and sealed. This loading procedure initially produced samples that were unsuitable for the experiment as there was a significant amount of dust contamination. The sample was then melted back until only a small amount of crystal was left. It was then left in the apparatus for about one month to allow the dust to settle to the bottom of the tube. The tube was then rapidly moved down in the temperature gradient. This caused the interface to move up rapidly and trap the impurities in a layer near the bottom of the crystal. A good optical quality interface was then be established. Before each run we scanned the interface to check for any sign of scattering from residual dust, and only proceeded with the run if the interface was clean.

3.3. Apparatus

3.3.1. General Description

The apparatus used in these experiments was essentially the same as that used by O. Mesquita for the experiments on salol and cyclohexanol.[36-39] However, there have been several improvements. A diagram of the general layout is given in Fig 3.3. A brief description follows, with most attention paid to the components that have been changed. For a more detailed description refer to the Ph. D. thesis of O. Mesquita.[86]

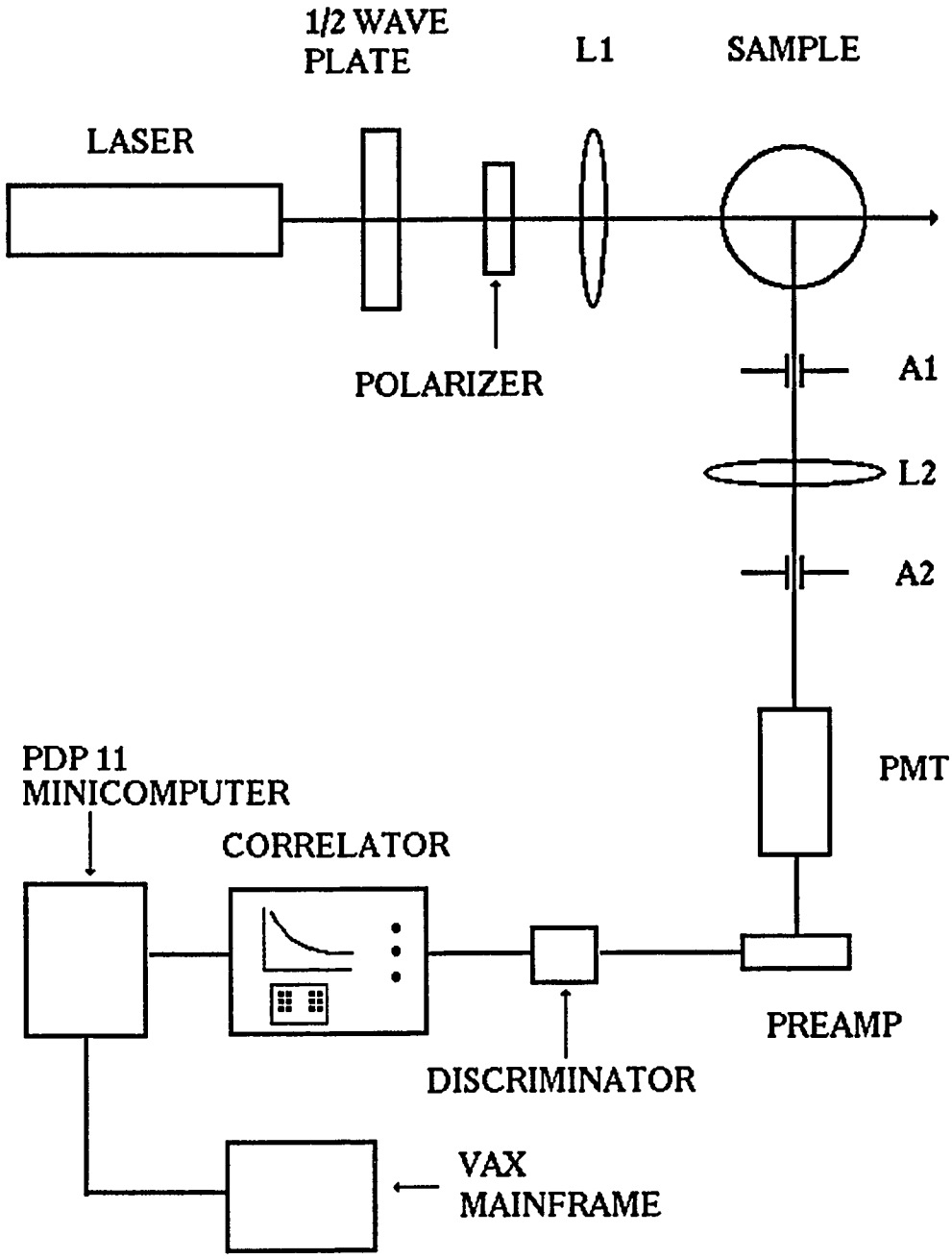

Fig 3.3: Schematic layout of apparatus.

The apparatus was mounted on a Modern Optics Vibration Isolation Table Model st-40E/s-4. The laser source was a Spectra Physics 165 argon ion laser, operating in single mode at λ=488 nm. The laser was focussed onto the interface by a 40 cm focal length lens. The collection optics consisted of a 1mm pinhole behind which an 18 cm focal length lens imaged the scattering volume onto a 100μm pinhole. The photomultiplier (PM) used to detect the signal was an ITT FW130. The output of the PM was amplified 10 times by a LeCroy preamplifier model A1007. The output was then passed to a discriminator and finally to the correlator. The correlator used in these experiments was a 144 channel Langley Ford model 1096. The last 16 channels can be delayed by an additional 1024 channels to establish the baseline of the correlation function. It is also equipped with a microprocessor to do local cumulants analyses, or the correlation data can be passed to an external device via a RS-232C data output. The sample time can be selected from 0.1μs to 9.9 sec. A precomputational delay of 1024 channels can be inserted before the first channel. The correlator can be run in either prescaling or clipping mode. The level ranges from 1 to 128 in powers of two. The correlator can be controlled externally via the RS-232C output. In our experiment the auotcorrelator was interfaced to a PDP 11 minicomputer. A program LCORIN was written in assembly language to control the correlator. LCORIN prompts the user for the file in which to store the data and asks the user to select the number of runs. It then starts the correlator. At the end of each correlation run the data was transferred to the PDP 11. The data file so produced is then transferred to the physics department's mainframe VAX computer for analysis. A Fortran program LFCOR2 in the VAX fits the data to Eq 2.24.

3.3.2. The Crystal Growth Chamber

The main crystal growth chamber consisted of two aluminum cylinders of height 4.5 cm and external diameter 10.2 cm, which constituted the hot and cold blocks, separated by a Lucite cylinder of height 4 cm and diameter 10 cm, which constituted

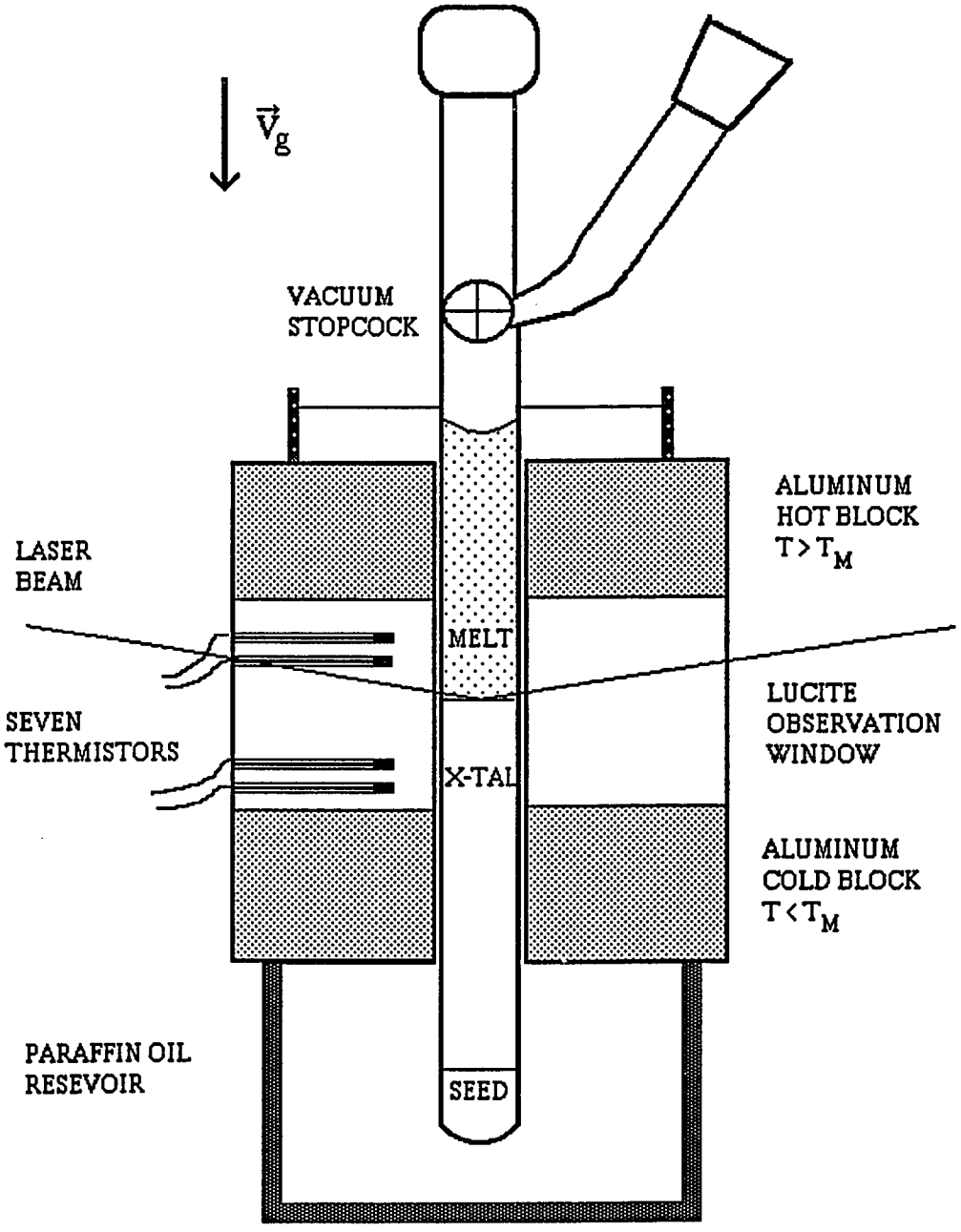

Fig 3.4: Crystal growth chamber

the observation window. The chamber is illustrated in Fig 3.4. All three blocks were drilled to a bore of 2.54 cm, to allow the growth tube to slide freely. The apparatus was filled with paraffin oil, to provide good thermal contact and also to provide refractive index matching. The temperature of the upper block was controlled by a YSI proportional thermister temperature controller model 72, which was connected to two cartridge heaters (Hotwatt inc) embedded in the block. The cold block temperature was controlled by water circulated by a Lauda Refrigerated circulator model K-2/R. The Lucite observation window design has been changed from the one used by Mesquita in the previous salol experiments. In order to improve the optical quality of the setup, the thin outer Lucite shell of the previous apparatus was removed along with the apparatus to blow warm air past the window (necessary for the previous apparatus to ensure the temperature in the thermostat monotonically increased from the cold to the hot block). Instead a much thicker piece of Lucite was used, ~ 10 cm instead of ~ 5 cm. The Lucite observation window was also made shorter to minimize the radial heat loss.

The temperature profile was measured by seven calibrated thermistors embedded in the Plexiglass cylinder spaced 0.5 cm apart; their resistance was monitored by an Omega automatic signal scanner model Dataplex-10. The temperature was displayed by an Omega digital temperature indicator Trendicator model 410-THC.

The vertical motion of the crystal was provided by a crystal pulling apparatus constructed in the physics department machine shop by R. Quinlan. The main drive screw is a precision stainless steel screw purchased from Winfred M. Berg Inc. The screw was driven by a synchronous motor equipped with a six speed gear selector (Inesco Co Model 06700-4S) attached to a second gear box (Inesco Co Model 00143). The various combinations of gear ratios provide 28 growth speeds varying from 0.00423 μm/s to 8.467 μm/s .

3.3.3. The Mass Spectrometer

The mass spectrometer used to analyze the gas present in the succinonitrile samples was an Extranuclear C50 quadropole system (Extranuclear Inc Pittsburgh, PA.), equipped with a vacuum system consisting of a turbomolecular pump and roughing pump. The gas analysis experiments were done in collaboration with Prof. Robert Graff of the Chemical Engineering Dept. of CCNY, in his laboratory.

3.4. Experimental Procedures

3.4.1. General Procedure

After the growth tube was placed in the crystal growth chamber the two aluminum blocks were heated. Typical block temperature values are: for salol, hot block temperature T_H=46.0°C, cold block temperature T_C = 37°C. For succinonitrile, T_H = 75°C, T_C = 20°C. The measured temperature profile in the thermostat is shown in Fig 3.5. As has been previously mentioned (see introduction Sec. 1.2) for strongly faceting materials such as salol there are two distinct scattering phenomena, one oscillatory and one diffusive. The choice of scattering geometry determines which process is observed.

To observe solely the oscillatory scattering one must scatter light off the interface, but minimize the light that passes through the melt immediately adjacent to the interface. This is done by totally internally reflecting the beam from the solid side of the interface. If the crystal is growing along the b-axis then this is possible for vertically polarized light (n_m= 1.598 n_b=1.83). The scattering is strongest when the $q_{||}$ vector is normal to the front of an advancing growth step that is propagating across the surface. Thus, one rotates the crystal about its axis until the scattering is seen.

To observe the diffusive scattering is a simpler matter as one merely has to bring the beam in from the liquid side. The diffusive scattering is considerably stronger than the oscillatory, and therefore dominates the correlation function. It is also possible

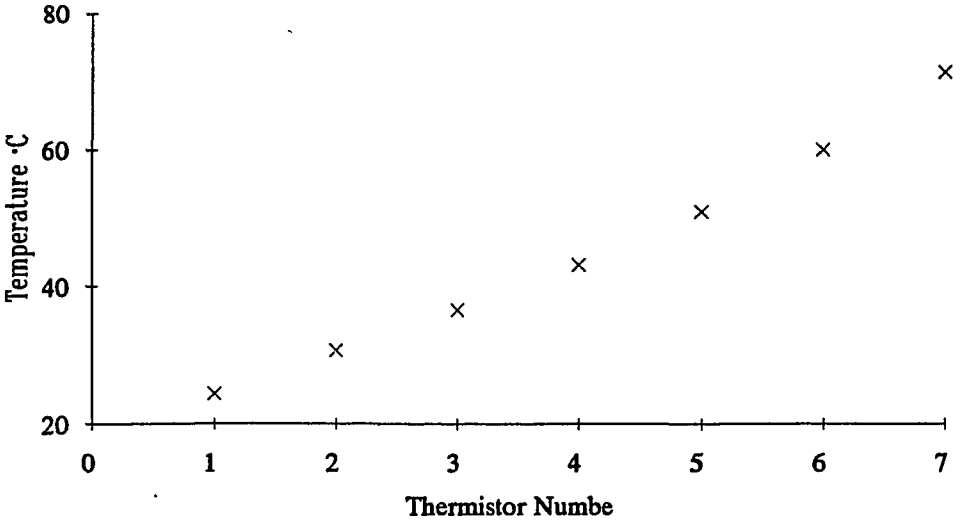

Fig 3.5: Temperature profile in the thermostat T_H = 77.41°C, T_C = 16.37 °C. The sample was succinonitrile

to observe the diffusive scattering if we bring the beam in from below, but horizontally polarized and with the a axis of the crystal in the plane of incidence (n_m= 1.598 n_a=1.66).

3.4.2. Long Time Evolution Studies of the Scattering in Salol

For the experiment on the long-time evolution of the scattering, the crystal was melted back to the seed to give us ~ 12 cm of melt. Growth was begun at 0.0423 μm/s and continued until a good optical quality flat interface was obtained. Growth was interrupted for 24 hours or so to allow any gasses that had built up in front of the crystal to diffuse away, and then resumed at our chosen velocity for that experiment. The growth velocities during the experimental runs were in the range v_g = 0.0847 μm/s - 0.212 μm/s. Temperature gradients were in the range 0.45 °C/cm - 1.1 °C/cm. Initially there would be a period of several hours when no scattering was observed. Then the scattering would start to appear in patches on the crystal surface,

and eventually spread over the entire interface. Once the scattering appeared we recorded the correlation function of the scattered light at regular time intervals as the crystal grew, for periods of up to fourteen days.

3.4.3. Measurements of the Angular Intensity Distribution I(θ) of Scattering in Succinonitrile

The purpose of this experiment was to determine whether the scattering observed in this material has an angular intensity distribution that is better characterized by Mie theory or Ornstein-Zernike (OZ) theory. It is easier to differentiate between

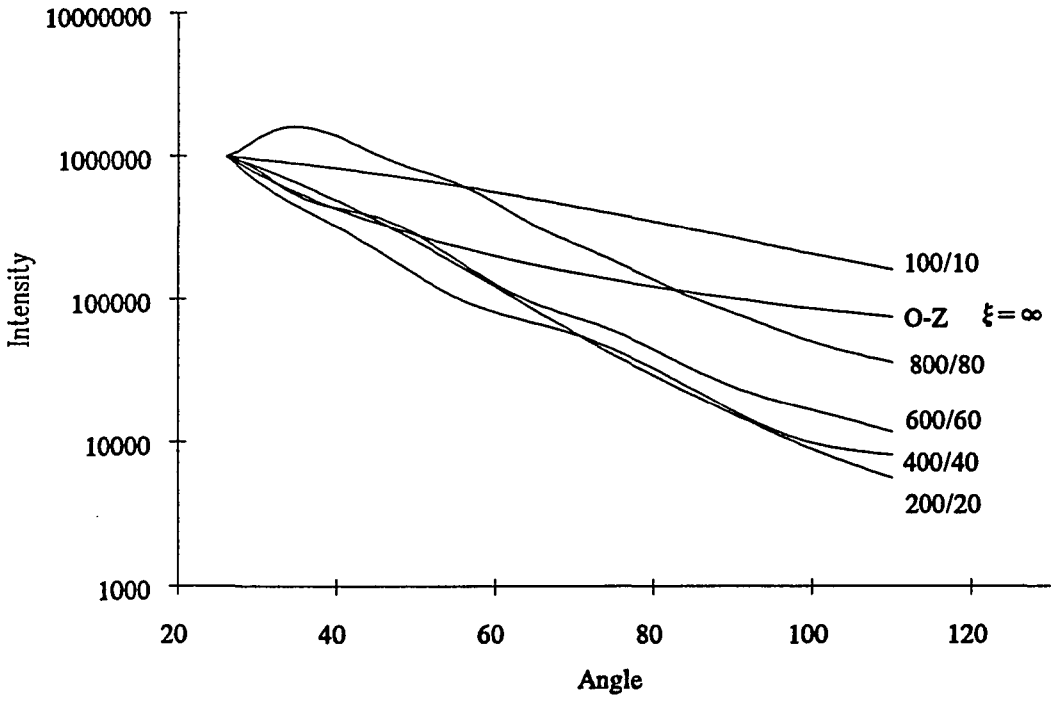

Fig 3.6: Angular intensity profile I(θ) for Mie and Ornstein-Zernike distributions. The Mie curves were generated for a Gaussian distribution of bubbles; the figures on the right refer to the mean and standard deviation of the distribution, both in nm. The single Ornstein-Zernike curve corresponds to a $\xi = \infty$. All curves are normalized to I(θ) $= 1.0 \times 10^6$ at $\theta = 26$ °.

these two forms of scattering if the characteristic length scale of the scatterers (i.e. the radius of the bubbles or the correlation length of the fluctuations) is in the range $0.2 < R < 0.6\ \mu m$. In Fig 3.6 we plot several theoretical predictions for Mie scattering and the OZ scattering prediction for $\xi = \infty$.

We can see from the plot that for bubbles in this range $I(\theta)$ decreases considerably faster with increasing θ than the Ornstein-Zernike curve for $\xi = \infty$. Note that the O.Z. $I(\theta)$ will fall off even less steeply for smaller values of ξ. Thus, the first step in this measurement was to find a succinonitrile sample where the radius extracted from photon correlation spectroscopy was in this range. The successful sample preparation procedure is described in Sec. 3.2.2.

The procedure followed to gather data was as follows. The sample was placed into the thermostat, and a temperature gradient of about 20 °C/cm was imposed. The sample was grown at a velocity $v_g = 0.339\ \mu m/s$. After about three hours when the surface was evenly scattering light we commenced taking data. The photomultiplier was rotated to the 20° position and the first point was taken. Each point was the average of two 40 second runs, where the total number of photo-counts was counted using the Langley-Ford correlator. The incident laser intensity was then adjusted to bring this reading to approximately 1.0×10^6 counts. This was done as a matter of convenience to enable us to easily compare different runs. Subsequent points were taken every 5° from 20° to 105°, the maximum angle possible with the apparatus. The points were not taken sequentially, but in a somewhat random fashion to minimize any possibility of systematic error. After all the data was collected the scattering angles were corrected to allow for the vertical component of the incident and scattered beam.

The scattering angle θ was calculated to be $\cos\theta = \cos^2\psi \cos\theta_{pm} - \sin^2\psi$, where ψ is the angle between the incoming beam and the surface of the crystal, and θ_{pm} is the angle through which the photomultiplier was rotated relative to the incident beam

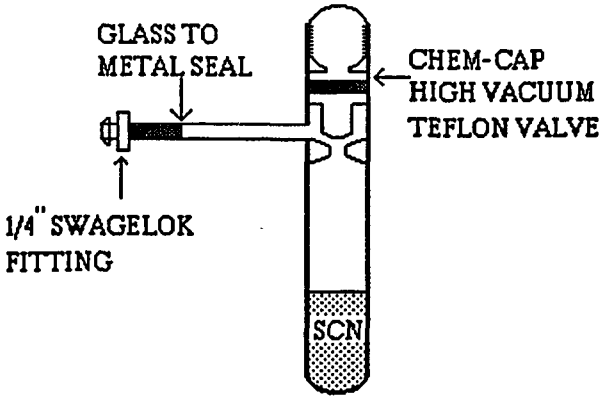

Fig 3.7: Sample cell for succinonitrile in gas identification experiment.

direction to collect the incoming signal. Prior to calculating θ, ψ was corrected for refraction at the Plexiglass air interface as the beam enters the thermostat.

It was verified that the scattering volume stayed constant as the scattering angle changed by observing the illuminated patch on the interface through the pinholes of the collection optics with a telescope. Even at 90° the entire illuminated volume could be sampled by the collection optics.

3.4.4. Identification of Gases Dissolved in Succinonitrile

A sample of succinonitrile (99% purity obtained from Fluka) was melted at atmospheric pressure and placed in an "Airfree" storage / reaction tube, (model number AF-0096-02 purchased from Chemglass, Vineland N.J.). This tube is equipped with a "Chem-cap" high vacuum Teflon valve designed for use down to 10^{-7} Torr. The tube had been modified by connecting a glass to metal seal on the inlet pipe, and then welding a 1/4" copper tube to the metal part. This enabled the tube to be connected to the mass spectrometer via a 1/4" swagelok fitting. The apparatus is illustrated in Fig 3.7.

The succinonitrile was allowed to solidify, and the gas collection tube was connected to the mass spectrometer. The Teflon valve was opened, and the gas

collection tube was evacuated with a roughing pump. The tube was further evacuated through the mass spectrometer using its internal pump, and a spectrum was taken of the solid succinonitrile. The Teflon valve was then closed and the succinonitrile was melted by immersing the gas collection tube in water at 80 °C. At this stage bubbles could be seen emerging from the liquid. After the succinonitrile was completely melted it was resolidified by immersing the gas collection tube in water at room temperature. The Teflon valve was opened again and another spectrum was taken. The two spectra were then subtracted to obtain the spectrum of the gas released by the bubbles.

3.4.5. Onset Measurements

It is well established that the diffusive scattering does not begin immediately when the crystal starts growing. There is always an onset time before scattering is observed. It has also been noted that the radius obtained from photon correlation spectroscopy is usually fairly constant for a particular sample from run to run. Thus, in these measurements we investigated the dependence of the onset time t_o and radius R_o on growth velocity.

Initially we tried to perform these measurement with a salol sample but were hampered by its slow growth kinetics. A crystal will not start to grow immediately after the crystal pulling motor is turned on. The interface must first reach a sufficient undercooling before growth begins. The crystal will therefore take a certain time for its growth rate to reach the rate at which the crystal is being pulled. For salol the time required for the crystal to reach the selected velocity was comparable to the onset time for the scattering. Therefore, the growth velocity was not constant and could not meaningfully be related to t_o and R_o. Thus, we switched to succinonitrile for these measurements as its fast growth kinetics make it a more suitable material.

The measurements were all performed at a temperature gradient of $\sim$ 20 °C/cm, and at growth velocities varying from 0.212 μm/s to 2.217 μm/s. The

crystal was grown until a good quality interface was obtained. The sample was then left for a few days to allow any gases that had built up in front of the crystal to diffuse away. The chosen velocity was then selected, and growth was started. The interface was then observed visually. The first appearance of visible scattering usually corresponds to the signal detected by the PMT being roughly twice the background signal of the light being scattered by the bulk melt. Once scattering was visible the onset time t_o was recorded. Several correlation functions were then taken to determine R_o.

4. RESULTS

4.1. Salol Results

4.1.1. General Scattering Characteristics

In our interfacial light scattering studies of salol both the oscillatory and diffusional scattering were observed. In a typical run, the weak oscillatory scattering could be seen ~ 30 minutes after growth had begun. See Fig. 4.1 (a). After 3-4 hours, patches of brighter diffusive scattering would appear on the surface of the crystal. Taking the correlation function with the beam coming on to the interface from above, one could now begin to see the exponential correlation function characteristic of the diffusive scattering. If the $q_{||}$ component of the scattering vector coincides with a normal to the face of a propagating growth step on the surface one can observe the exponential relaxation building up under the oscillatory component as shown in Fig. 4.1 (b). Eventually, after about 24 hours the patches would have spread across the entire interface. The diffusive scattering, which becomes much more intense than the oscillatory scattering, then completely dominates the correlation function as shown in Fig. 4.1 (c). The diffusive correlation functions typically had an A/B ratio of 0.7 and a polydispersity of about 0.3.

The time for onset of the diffusive scattering and the scattering intensity are extremely dependent on the sample preparation and growth conditions. If samples were very carefully multiply distilled and grown from clean seed crystals, the diffusive scattering would not appear at all, even after many hours of growth. It was also noted that the scattering intensity diminished and the bubble size grew larger, if the crystal was repeatedly grown from the seed to the end of the growth tube and then melted back to the seed and regrown. Presumably, this was due to the gas segregated at the interface not being reabsorbed back into the melt once the bubbles had passed out of the region of high gas concentration near the interface.

It was found that bubbling nitrogen or helium through the samples did not

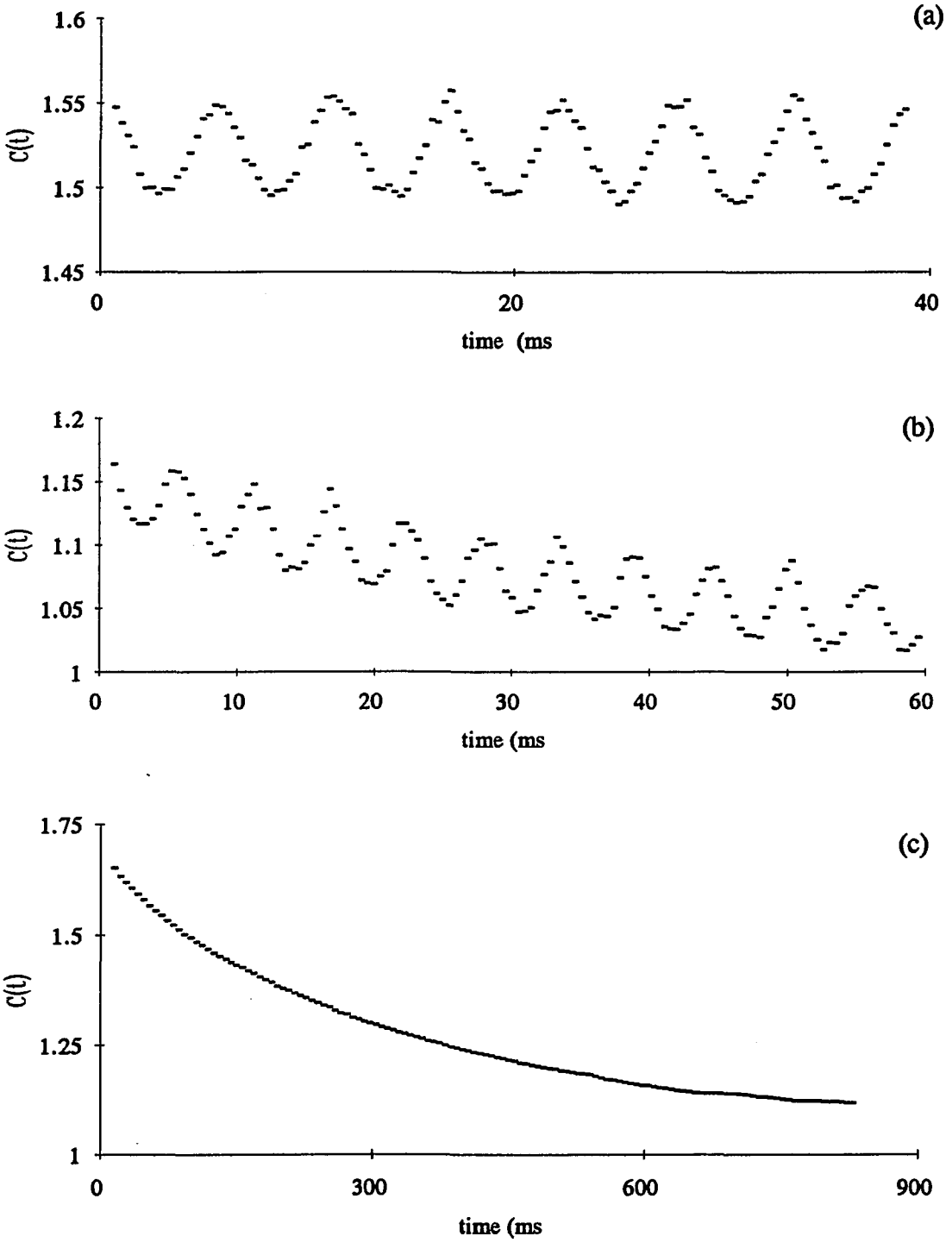

Fig 4.1: Reduced intensity autocorrelation function for light scattered at the crystal-melt interface of salol. (a) 30 minutes , (b) 3-4 hours, and (c) 24 hours after initiation of growth.

significantly enhance the scattering which suggests that the gas in the bubbles did not readily dissolve into the melt. Further, the scattering was also seen to persist for many hours after growth had stopped. These two observations suggest that the bubbles are more stable, with respect to the diffusion of gases across their surface and into the melt, than a simple model such as that of Epstein and Plesset[76], which predicts lifetimes of the order of a few seconds for bubbles in undersaturated solutions. (see Table 2.1.)

4.1.2. Long Time Evolution of Scattering in Salol

For runs extending over a period of fourteen days or so we generally found an initial radius of ~ 1 μm that would increase continuously (with fluctuations) to a final radius of ~ 100 μm as illustrated in Fig 4.2. We also noted that the polydispersity, as extracted from the correlation function, increased from an initial value of ~ 0.3 to a final value of ~ 1 - 2. Although the growth velocity was low, the initial diffusion constant D ~ 0.4 $\times 10^{-9}$ cm^2/s agreed with values found at larger velocities in the experiments of Durig *et al.*[29] and Mesquita *et al.*.[36] Note that in this experiment the onset of scattering required ~ 25 hours.

On two occasions the bubbles became large enough to be trapped by the advancing interface. After trapping a layer of bubbles, we allowed the crystal to solidify completely and then removed it from the thermostat and examined it under a microscope. This permitted the first direct visualization of the microbubbles; a photograph is shown in Fig. 4.3. We were also able to measure the radius of the bubbles directly. The result (R= 50 - 100 μm, at v_g=0.212 μm/s) agrees well with the empirical relation of particle size to growth velocity for the capture of inclusions found by Chernov and Temkin's survey.[82] This result is illustrated in Fig 4.4. taken from their survey, which shows experimental data from several different experiments on the trapping of particles, along with theoretical curves. Our data has been added to the

figure and is represented by the large cross. In their article[82] Chernov and Temkin noted that the whole data set may be roughly approximated by the relation $V_C = E/R^m$ where m = 1-2.

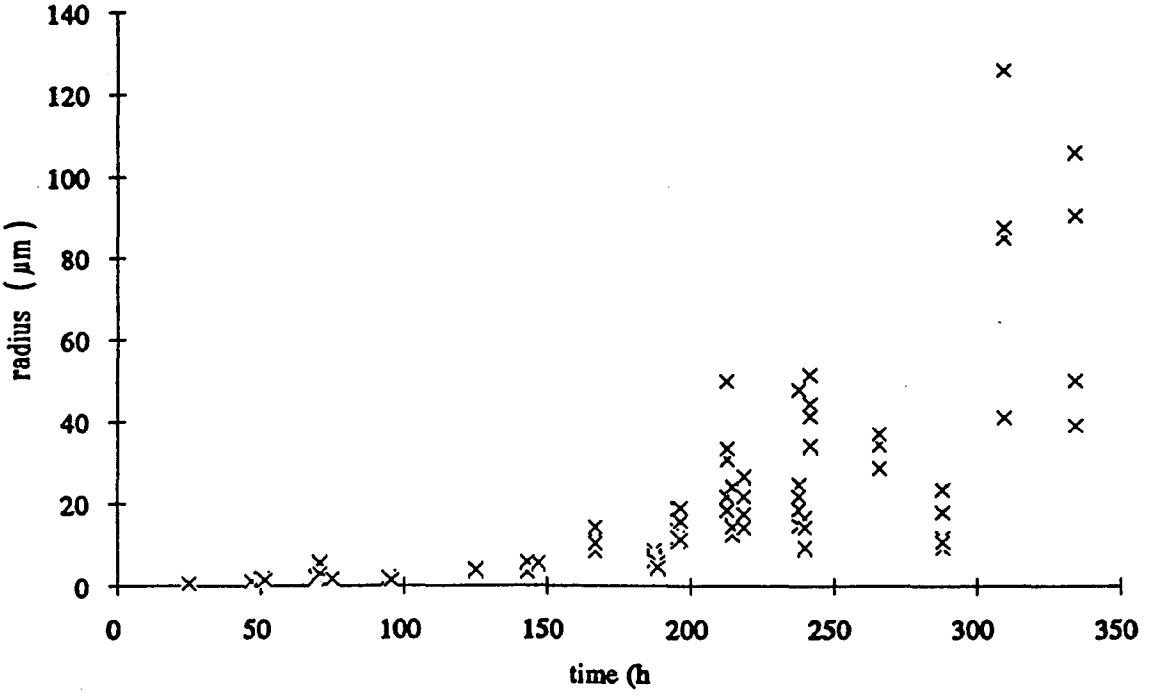

Fig 4.2: Radius of bubbles in salol vs time after growth was initiated. Growth velocity v_g=0.00847 μm/sec. Temperature gradient G = 1.1 °C/cm

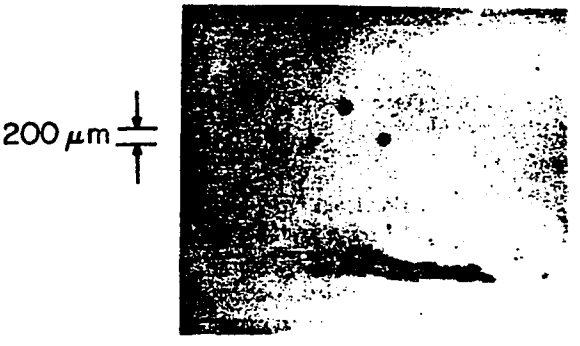

Fig 4.3: Photograph showing bubbles that have been trapped in salol by the advancing crystal interface.

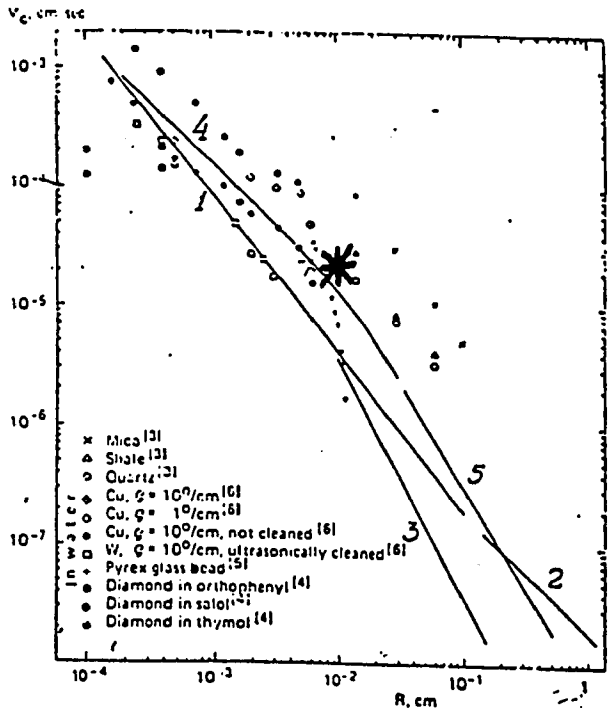

Fig 4.4: Figure From Chernov and Temkin's survey.[82] Our data has been added as the dark cross.

4.2. Succinonitrile Results

4.2.1. General Scattering Characteristics

As succinonitrile is a nonfaceting material with a surface that grows atomically rough, only the diffusive scattering could be seen. The diffusion coefficient extracted from the correlation functions, for the sample used for the angular intensity measurements, was $D \sim 3 \times 10^{-9}$ cm^2/s. This corresponds to a bubble radius of $R \sim$ 430 nm, or a correlation length of $\xi \sim 290$ nm. The polydispersities were $\mu_2/\Gamma^2 \sim$ 0.4. A typical correlation function is plotted in Fig 4.5. For the sample used in the onset measurements the bubble radius was $\sim 4\ \mu$m, and the polydispersities were again $\sim$ 0.4.

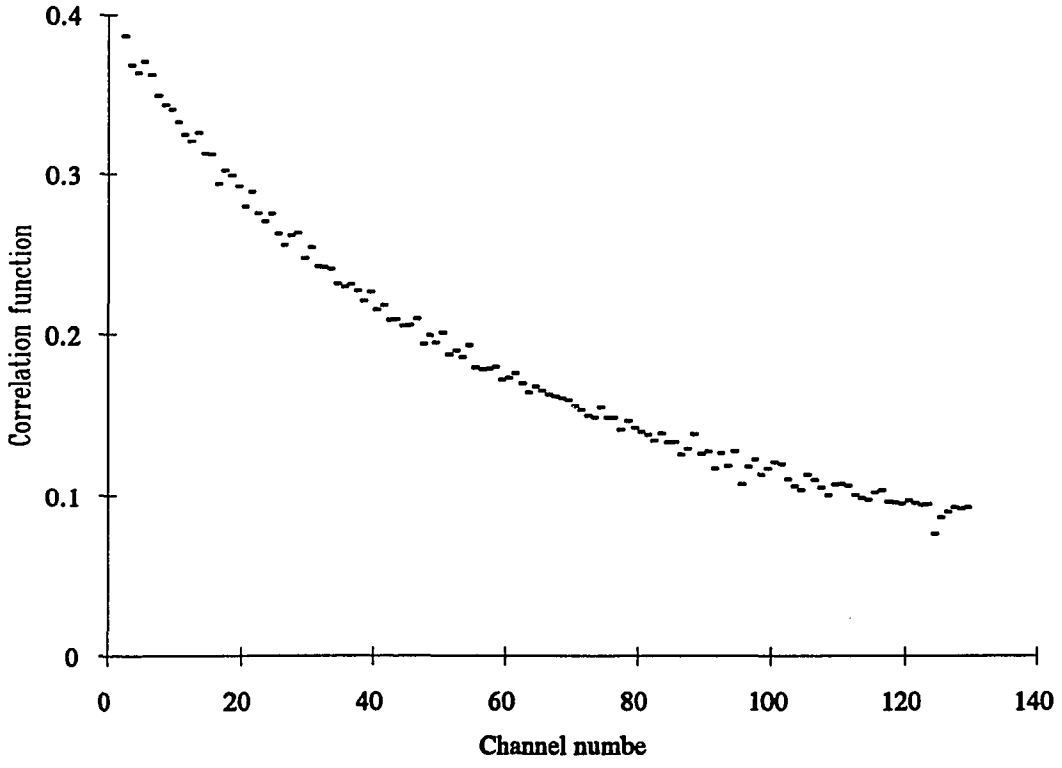

Fig 4.5: Correlation function ($C(\tau) - C(\infty) / C(\infty)$) of light scattered from surface of a succinonitrile crystal.

4.2.2. Measurement of Angular Intensity Distribution in Succinonitrile

In Fig 4.6 we plot the results of a single measurement of the angular intensity $I(\theta)$. The solid line represents a fit of the data with Mie theory. A program was written that generates the Mie function in Eq 2.28 for a Gaussian distributions of bubble scatterers. Angular scattering functions for various combinations of mean radius R_{av} and standard deviation σ_R were generated and compared to the data. The line shown represents the nearest match found, and corresponds to a mean radius $R_{av} = 475$ nm and standard deviation $\sigma_R = 47.5$ nm. The dashed line represents the closest possible

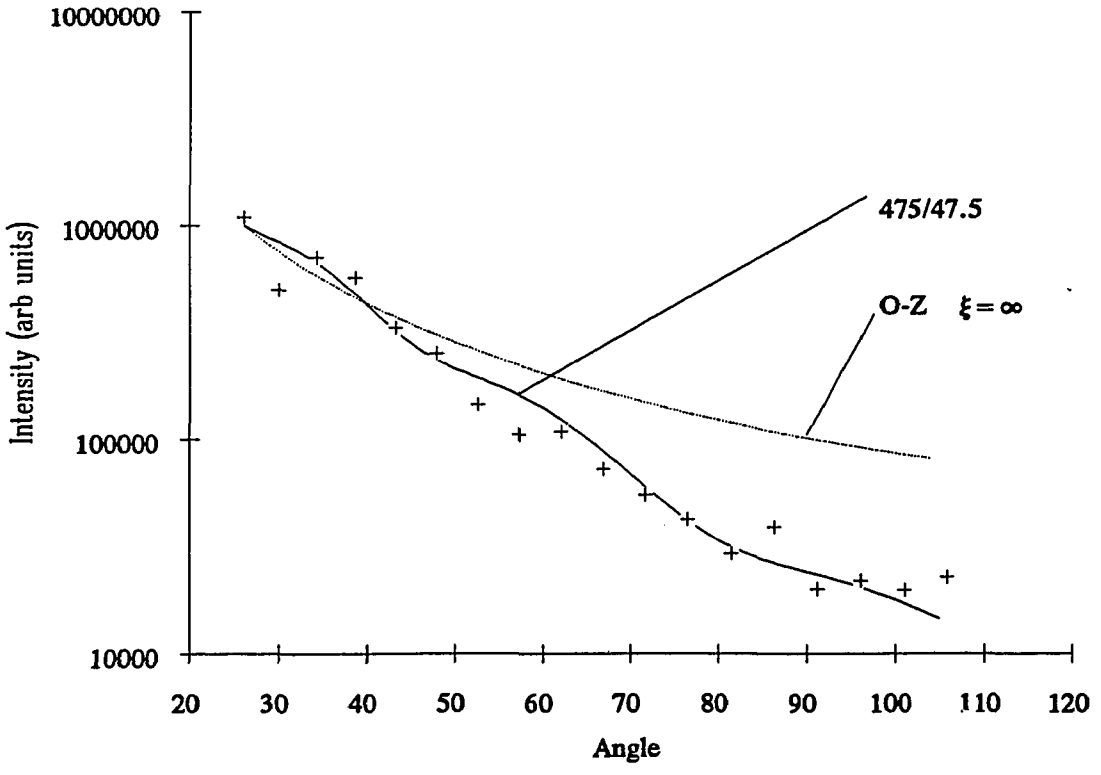

Fig 4.6: Scattered intensity vs angle θ for light scattered from the interface of growing succinonitrile crystal. Radius of scatterers extracted from dynamic light scattering measurement $R \sim 430$ nm. The solid and dashed lines are theoretical predictions for Mie theory and OZ theory.

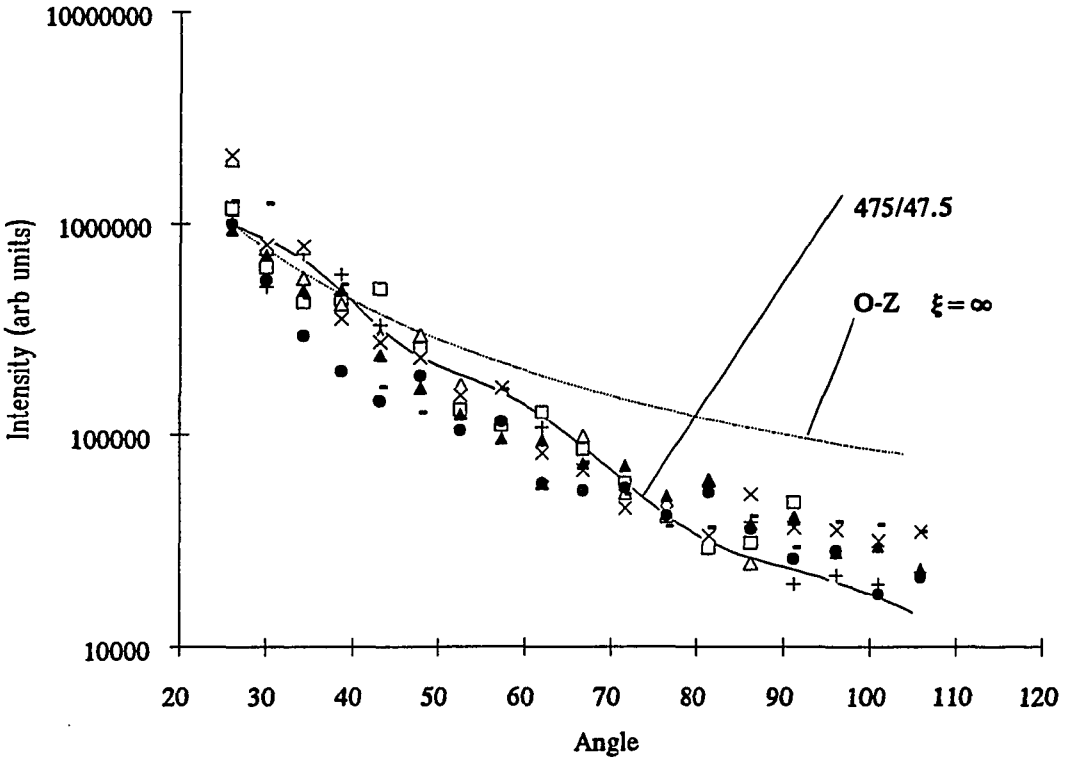

Fig 4.7: Scattered intensity vs angle for all seven measurements performed. Again plotted with the best Mie fit to the data (R_{av} = 475 nm R_{σ} = 47.5 nm), and the $\xi = \infty$ Ornstein Zernike theoretical curve. In all cases the radius extracted from the dynamic light scattering measurements was R ~ 430 nm.

fit of the data with Ornstein-Zernike theory. Curves of $I(\theta) = I_o(1 + q^2(\theta)\xi^2)^{-1}$ were generated for various values of ξ. For all values of ξ, the predicted $I(\theta)$ falls of too slowly with increasing θ to enable the data to be well fitted (note that reducing ξ to any finite value makes $I(\theta)$ fall off more slowly). Both theoretical curves are normalized to 1.0×10^6 at $\theta = 26$ °. From this figure it is quite clear that Mie theory provides a much closer match to the data than Ornstein-Zernike theory.

Upon closer examination of the data, one can see that although the Mie function is clearly a reasonable fit, it is not an ideal fit. For large angles the experimental data is somewhat above the Mie curve. This was a common occurrence when we tried to fit the data. In all, seven runs were performed, and these are all plotted in Fig 4.7. It is possible that the scattering sample contains a certain number of small bubbles that contribute to the scattering at larger angles. In any case the Gaussian distribution we employed in computing the theoretical curves should be viewed as a rough approximation to the actual distribution which is unknown.

4.2.3. Measurements of the Onset Time and Radius

In the microbubble model the delay between initiation of crystal growth and the onset of scattering is attributed to the time necessary for the gas concentration at the interface to build up to the level necessary for nucleation. Pohl[87] has solved the full time dependent diffusion equation, Eq. 2.79, for the solute concentration C ahead of a planar interface. The solution valid for small k is

$$\frac{C(z,t)}{C_o} = 1 + \frac{1-k}{k}\left[e^{-\frac{v_g z}{D}} - e^{-\frac{v_g}{D}(1-k)(z + kv_g t)} \right] \qquad (4.1)$$

where C_o is the background concentration of gas in the melt, k is the segregation coefficient in the melt and v_g is the growth velocity and D is the diffusion coefficient of the gas in the melt. Thus, the concentration at the interface $C_i(t)=C(z=0,t)$ follows the time dependence.

$$\frac{C_i(t)}{C_o} = 1 + \frac{1-k}{k}\left[1 - e^{-v_g^2 \frac{(1-k)k}{D} t} \right] \qquad (4.2)$$

Eq. 4.2 can be used to estimate the characteristic time constant t_{eq} for the buildup of gas at the interface.

$$t_{eq} = D/[(1-k)kv_g^2] \qquad (4.3)$$

If we assume that k is in the range[47] $0.01 < k < 0.1$ and $D \sim 10^{-5}$ cm^2/sec, and calculate Eq. 4.3 for the fastest and slowest growth velocities that were used it is found that for $v_g = 2.12$ μm/s $t_{eq} = 43$ mins., and for $v_g = 0.212$ μm/s $t_{eq} = 4300$ mins. For the slowest velocity t_{eq} is two orders magnitude longer than the onset time t_o observed. For the fastest velocity t_{eq} is $\sim$ 5 times longer than the onset time t_o. Therefore, it is a reasonable approximation to expand the exponential in Eq. 4.2 and keep only the first order terms. Doing this it is found that

$$\frac{C_i}{C_o} \approx 1 + v_g^2 \frac{(1-k)k}{D} t \approx 1 + \frac{kv_g^2 t}{D} \tag{4.4}$$

If the bubbles nucleate at the gas concentration C_i their radius is given by Eq 2.83 as

$$R_o = \frac{2\sigma}{P_l \left[\frac{C_i}{C_o} - 1\right]} \tag{4.5}$$

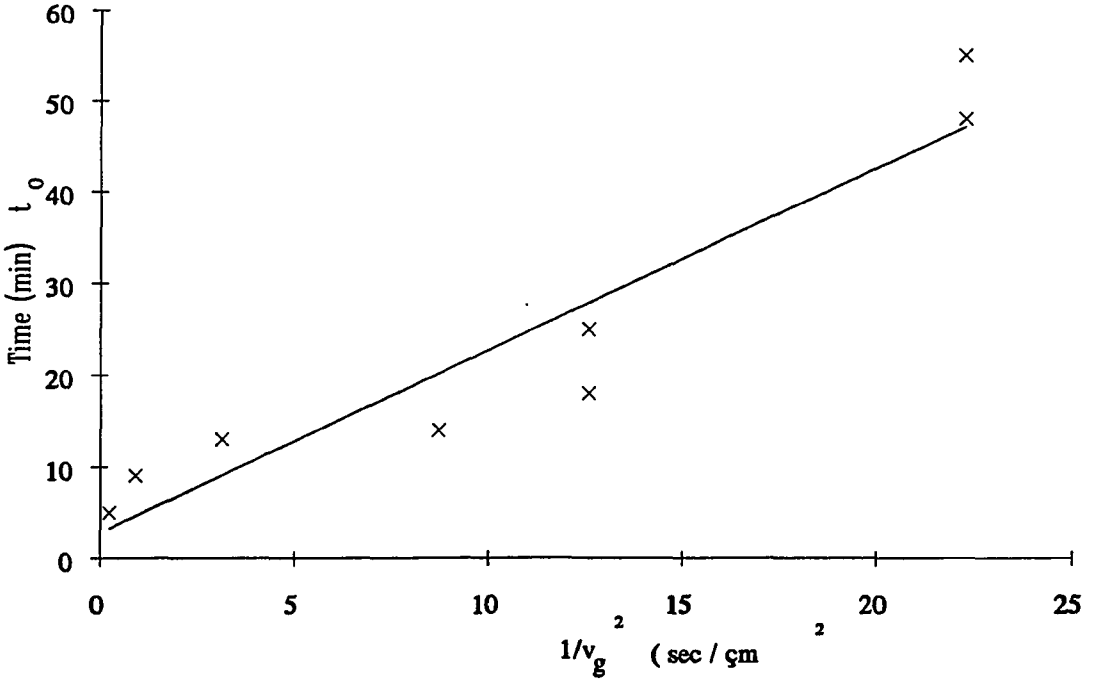

Fig 4.8: Time for onset of scattering (minutes) vs the inverse square of the growth velocity (μm/sec). The solid line represents a linear fit through the data.

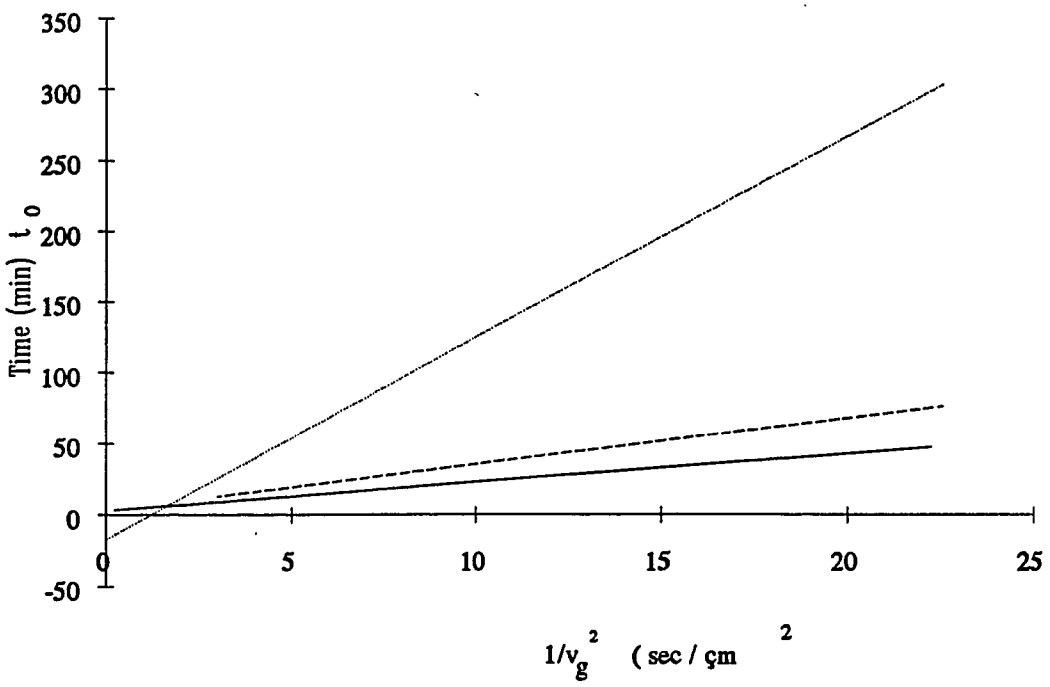

Fig 4.9 : Onset time t_o (in minutes) vs inverse square of growth velocity v_g (in μm/sec). The solid line represents a linear fit to the data. The dashed line corresponds to the results of Laherrere *et al.*[48] before pumping on the succinonitrile, and the dotted line to the results of Laherrere *et al.*[48] after pumping.

where C_s is the saturation concentration of the melt. If we assume $C_o \sim C_s$ then Eqs. 4.4 and 4.5 can be equated and we find

$$R_o t_o \approx \frac{2\sigma D}{P_o} \frac{1}{v_g^2} \qquad (4.6)$$

Mesquita *et al.*[44] have observed a systematic variation in both R_o and t_o with growth velocity v_g in their experiments. However, we saw no systematic variation in R_o, only in t_o. In Fig 4.8 we plot t_o vs $1/v_g^2$. The line represents a straight line fit through the data. From the Figure we see reasonable agreement with Eq. 4.6. We notice a positive intercept on the time axis of $\sim$ 3 minutes which we interpret as a result of the time lag between the crystal pulling motor starting, and the interface reaching

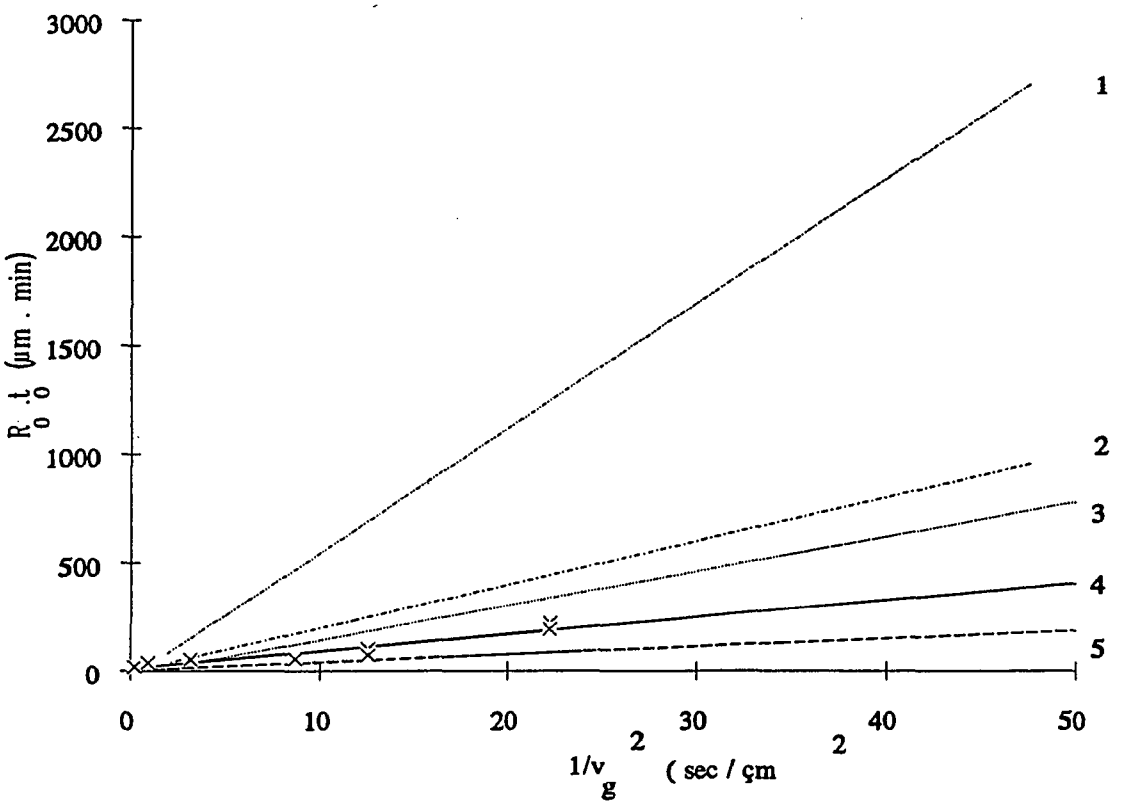

Fig 4.10: Onset radius $R_o(\mu m)$ times onset time $t_o(min)$ vs inverse square of growth velocity $v_g(\mu m/sec)$. Linear fits to data: (1) naphthalene Mesquita *et al.*[44], (2) Biphenyl Mesquita *et al.*[44], (3) Succinonitrile (Laherrere *et al.*[48] after pumping), (4) Succinonitrile (This work), (5) Succinonitrile (Laherrere *et al.*[48] before pumping). Crosses, data this work.

the steady state undercooling necessary to achieve a growth velocity of v_g.

In Fig 4.9 we compare our measurements to those of Laherrere *et al.*[48] (also performed on succinonitrile). In Fig 4.10 we plot $R_o \cdot t_o$ vs $1/v_g^2$ and compare our data to the results of Mesquita *et al.*[44] for naphthalene and biphenyl, and of Laherrere *et al.*[48] for succinonitrile (for our data we take $R_o = 4\ \mu m$, for Laherrere *et al.*[48] $R_o = 1.125\ \mu m$. These were the average values found from the autocorrelation measurements).

From Fig 4.9 we note that our onset times were comparable to those Laherrere *et al.*[48] obtained before pumping on the sample. However our onset radius was ~ 4 times larger. This suggests that if we utilize Eq 4.5, the C_i for our sample was smaller than theirs. One can further infer that as the time for onset was similar in both cases, the values of C_i/C_o (from Eq 4.4) for the two samples were similar. This suggests that the sample of Laherrere *et al.*[48] had a larger background gas concentration C_o than ours. These differences in the samples can be understood if we consider the different ways in which the samples were prepared.

The sample of Laherrere *et al.*[48] was <u>not</u> distilled, but zone refined many times. Our sample was distilled but not zone refined. It is quite possible that the gas may not be efficiently segregated by the zone refining, or that once it is segregated it may redissolve in the solid. However, it is well known that distillation is a common, if not perfect, way of degassing materials. Thus, it is quite probable that distilled samples will have lower gas concentrations than zone refined samples. This is quite consistent with our experiences with both succinonitrile and salol, that if samples are very carefully multiply distilled the diffusive scattering phenomena goes away. This result has been also noted by Ladeira and Mesquita.[46]

The differences in initial gas concentration may also explain why bubbles in the sample of Laherrere *et al.*[48] nucleated at a smaller radius. If one supposes that there is a material dependent supersaturation C_N at which the gas concentration in the melt is sufficiently high that there is a reasonable probability that an observable number of bubbles would nucleate (e.g. one bubble per mm^3 per second), then one would expect that as the sample solidified the concentration at the interface would build up until $C_i=C_N$ and then nucleation would occur. In this case the onset radius would always be the same, only the onset time would be longer for samples with a smaller initial concentration C_o. However, this may only be true for samples were C_i increases slowly enough so that C_i does not change appreciably during the onset of nucleation. It

can be seen from Eq 4.4 that the rate of change of C_i, $\frac{\partial C_i}{\partial t} \propto C_o$. Thus, if a sample has a high initial concentration it is possible that C_i may be increasing so rapidly that it may overshoot C_N before an appreciable number of bubble nucleate and thus the main bubble nucleation will occur at a higher supersaturation. In this case the onset radius may be higher for samples with a higher initial concentration C_o. This may also explain why in the experiment of Mesquita *et al.*[44] a decrease in the onset radius with increasing velocity was observed as $\frac{\partial C_i}{\partial t} \propto v_g^2$.

An alternative explanation for the variation in onset radius between samples of the same material may have its origin in the heterogeneous nucleation process. It is possible that differing samples may have slightly different impurities, that on a microscopic level alter the number and nature of the heterogeneous nucleating sites at the interface. This may lower the nucleation barrier for some samples more than others, and lead to a variation in the onset behavior of the samples. This idea is discussed further in Sec 5.3.

4.2.4. Identification of Gases Dissolved in Succinonitrile

In the experiments on analyzing the gas dissolved in the succinonitrile by mass spectroscopy, the sample of succinonitrile was pumped on for several hours and a spectrum was taken. This spectrum is shown in Fig 4.11. The main peak at around 18 mass units corresponds to water. The smaller peaks at 28 and 32 mass units correspond to N_2 and O_2. The peaks at 54 and 80 mass units correspond to succinonitrile. After the gases were released from the succinonitrile a further spectrum was taken. This spectrum is shown in Fig 4.12. To obtain the spectrum of the gases we subtracted the first spectrum from the second. The result is shown in Fig 4.13. This spectrum is magnified ten times in Fig 4.14. The main peaks in order of decreasing size, and the components we attribute them to are given in the Table 4.1 below.

In the subtracted spectrum we see the succinonitrile peaks at 54 and 80 mass units present in the initial spectrum are no longer present. This is a useful check that the sensitivity of the spectrometer did not change between taking the first two spectra.

We can also see that the main gases released from the succinonitrile have an essentially air like composition. This can be seen by comparing our subtracted spectrum to the air spectrum in Fig 4.15. The slight differences in the ratios of the peak heights can be attributed to the different solubilities of the various components of air in succinonitrile.

Laherrere *et al.*[48] have suggested that the gaseous impurity that causes the segregation of bubbles at the interface of succinonitrile is methanol. We found no significant evidence for methanol in our spectra. A spectrum of an air sample with a small amount of methanol impurity in is shown in Fig 4.16. A signature of the presence of methanol is a peak at ~ 31. There is no significant peak at 31 in our subtracted spectrum. Thus, we conclude that for our succinonitrile methanol is not a the major gaseous impurity, although, it may be present in the succinonitrile used by Laherrere *et al.*[48].

That the main gaseous impurity is something as commonplace as air is quite reasonable as the dynamic scattering at the interface seems to be an almost universal phenomenon in crystal growth.

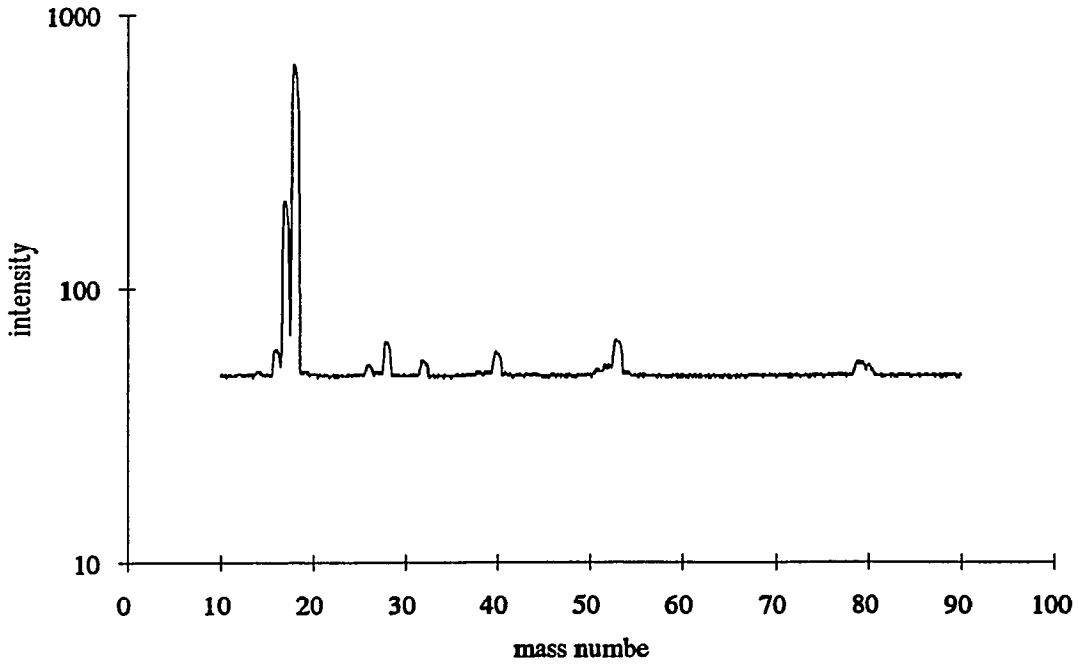

Fig 4.11: Spectrum of solidified succinonitrile sample before gas is released.

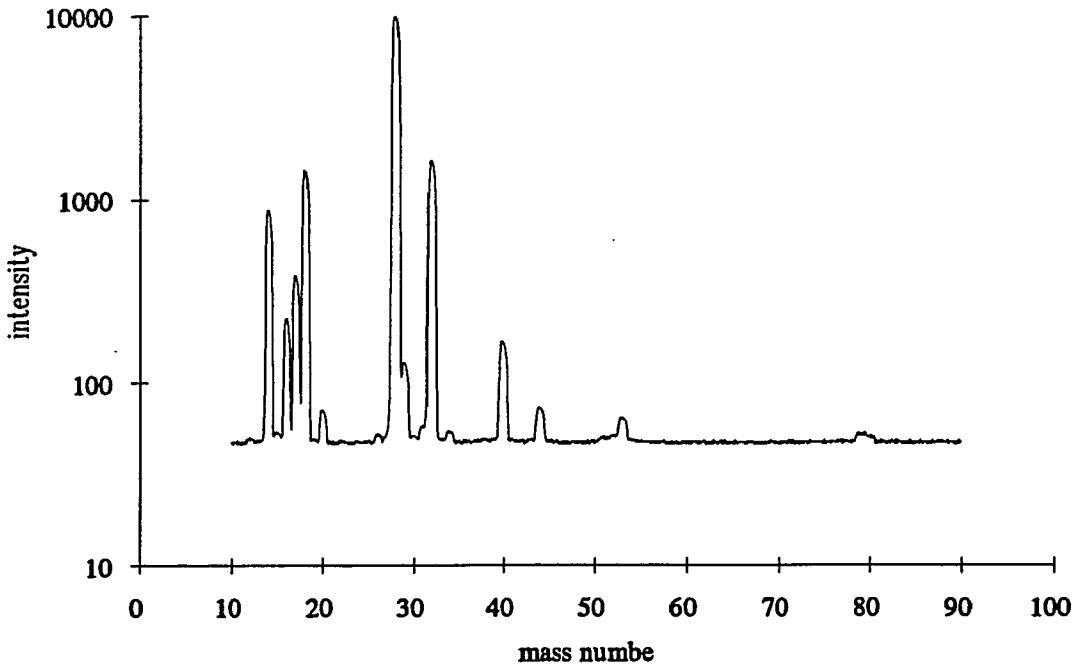

Fig 4.12: Spectrum of succinonitrile sample after gas is released.

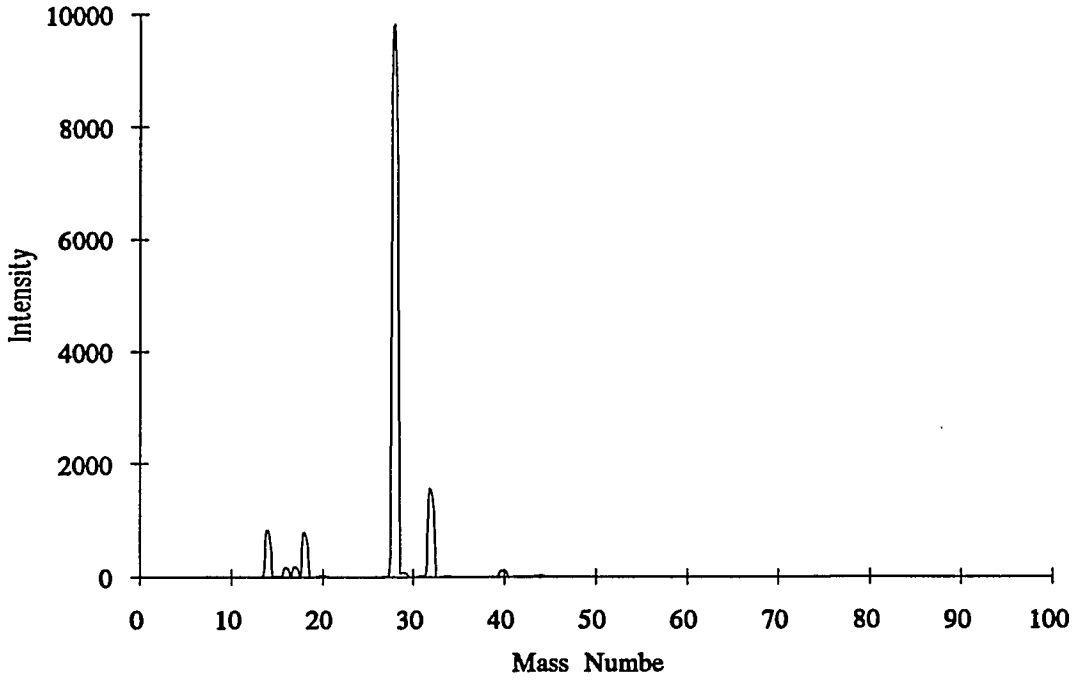

4.13: Subtracted spectrum constructed by taking the difference between the previous two spectra

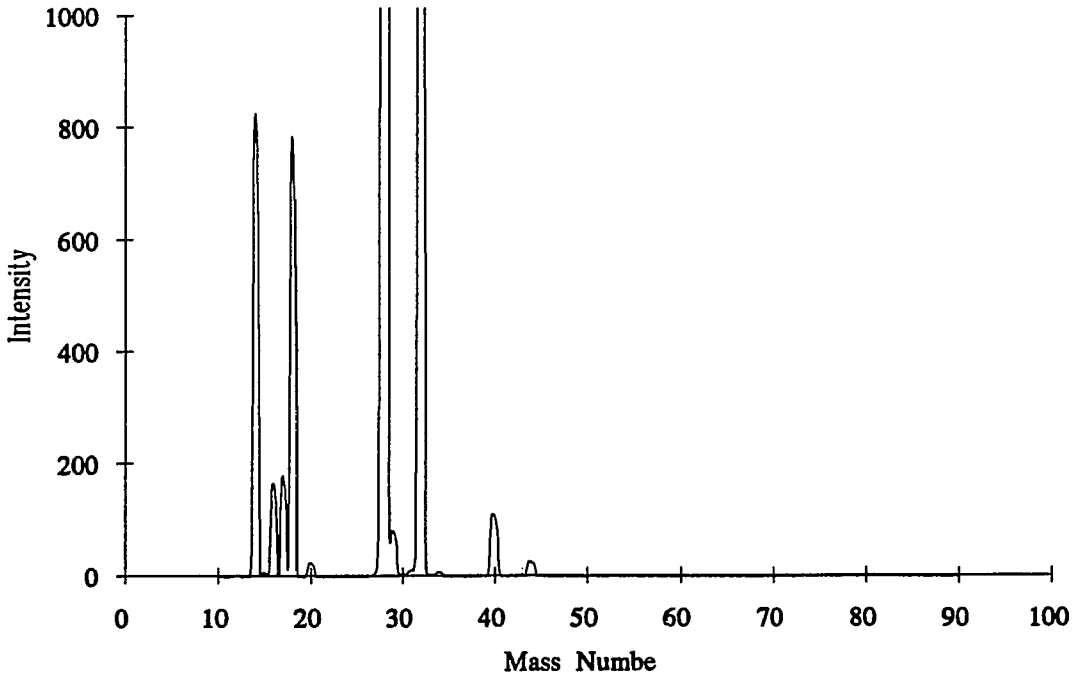

4.14: Subtracted spectrum magnified ten times to show detail.

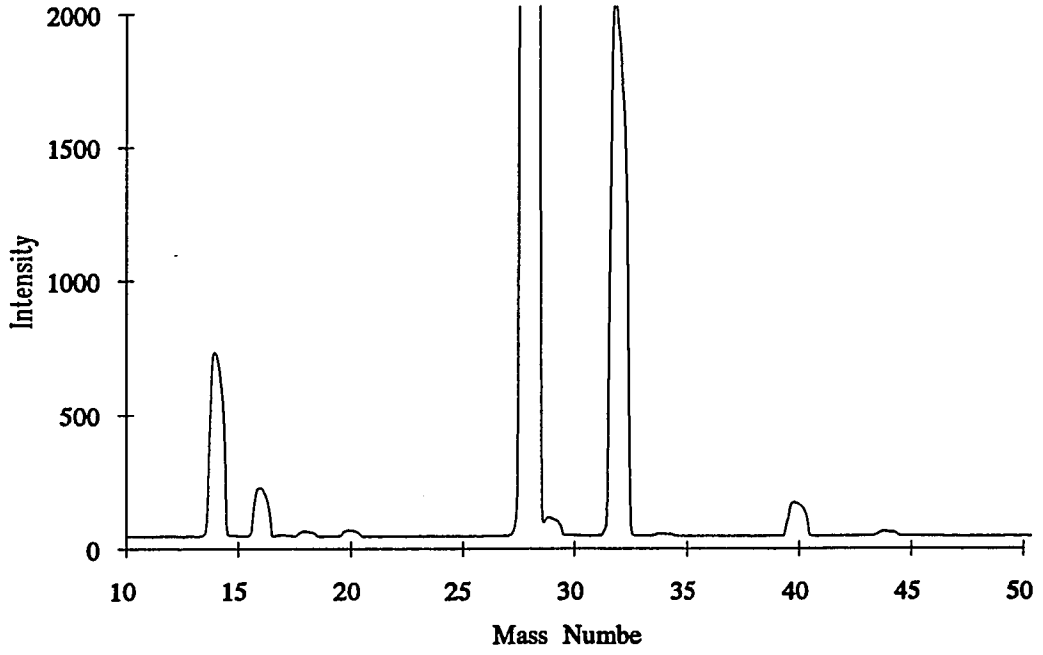

4.15: Spectrum of air.

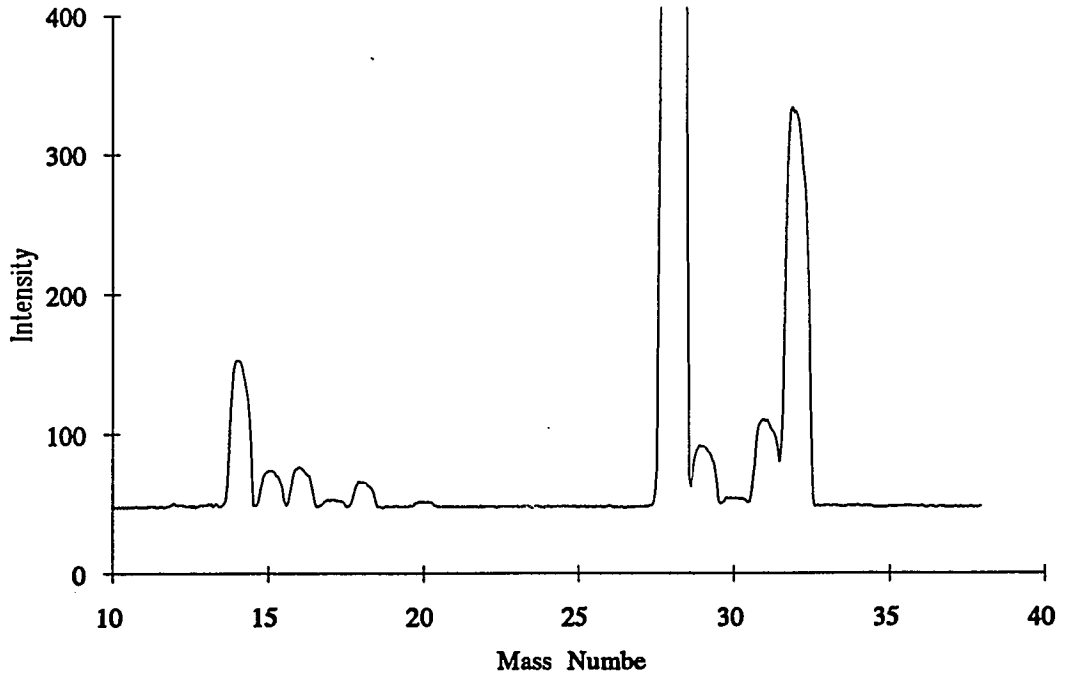

4.16: Spectrum of air plus a small trace of methanol impurity.

Location of peak	Peak height	Identification (mass)
27.95	9834	$N_2(28)$
31.80	1562	$O_2(32)$
13.95	824	N(14)
17.90	775	$H_2O(18)$
16.95	178	$OH^-(17)$
16.00	164	O(16)
39.75	109	Ar(40)
43.80	24	$CO_2(44)$
19.90	22	Ne(20)

Table 4.1: Positions of main peaks in the gas spectrum of Fig 4.13 and 4.14 along with their intensities and identification of probable origin.

5. DISCUSSION

5.1. The Origin of the Diffusive Scattering: Microbubbles or Mesophase

The microbubble model[38] explanation of the origin of diffusive scattering at the crystal melt interface has several attractive features. It provides a mechanism for generating scatterers (bubbles) at the interface that have a reasonably narrow size distribution. The diffusive motion of the bubbles provides an explanation for the correlation function of the observed light scattering. It also explains the long onset time for the scattering, since the buildup of excess dissolved gas concentration is a slow process at the low growth speeds employed. The narrowness of the scattering layer is then due to the exponential decay of the gas concentration with distance from the interface as predicted by Eq.2.82 and shown in Fig. 2.5. It also suggests why the observed diffusion coefficient D and polydispersity Q vary slightly from system to system, since the balance of transport and solute rejection and the nature of the heterogeneous nucleation process would both be expected to change from sample to sample.

There is now also a substantial body of experimental evidence for the microbubble model.[38] Perhaps the strongest is the direct visual observation of bubbles reported in this thesis. Further support for the model is provided by the observation that pumping on the system has a dramatic effect on the scattering. Our group has shown that by prolonged pumping on salol the scattering can be made to disappear.[40] Laherrere *et al.*[47] have shown that after repeatedly melting, recrystallizing, and pumping on the sample the scattering intensity decreased dramatically, and the bubble size increased.

In an experiment that is somewhat the converse of the previously mentioned one Vesenka and Yeh[42] have shown that injecting helium into the melt strongly enhances the scattering. They have also shown that the bubble size decreases with positive gas pressure.

An additional aspect of the phenomena that only readily finds an explanation in the microbubble model is that upon rapidly remelting the crystal after scattering has begun, the scattering layer detaches from the surface of the crystal and floats in the melt. This scattering layer persists for some time, and gradually spreads out before disappearing. This "lift off layer" can be easily understood as a consequence of the very small diffusion constants of the bubbles. This "lift off" phenomenon has been observed in the ice-water experiments of both Vesenka and Yeh[43] and Halter *et al.*[32], and in experiments performed at CCNY on cyclohexanol[39] and succinonitrile (observed during the course of this work).

Further evidence for the microbubble model[38] comes from the experiments on the onset of scattering by Mesquita *et al.*[44], Laherrere *et al.*[48], and this group. In all three experiments, the onset behavior was seen to follow the predictions of the microbubble model (described by Eq 4.6).

Additional evidence comes from analysis of the ETH group's data on the ice-water system. Firstly, their measurements of the thickness of the scattering layer show that it scales with the inverse of the growth velocity.[32] This is what the microbubble model would predict as the width of the high gas concentration layer in the melt scales as v_g^{-1} (see Eq 2.82). Secondly, Mesquita *et al.*[44] have analyzed the measurements of Böni *et al.*[28] of the increase in scattering intensity I and decrease in the linewidth Γ as scattering onsets. Mesquita *et al.*[44] have found that the data can be explained in terms of an increase in bubble size, if the radius extracted from Γ is used to calculate $I(\theta)$ with Mie theory.

We believe that we are now in a position to be able to answer the most serious objections to the microbubble model. The most recent challenge to this theory came from Steininger and Bilgram's measurements of the angular intensity $I(\theta)$ in cyclohexane.[33] In this measurement they state that $I(\theta)$ could only be fit by the Ornstein-Zernike theory of scattering from thermodynamic fluctuations, and could not

be fit by the Mie theory of scattering from spherical objects. However, there are now several measurements of I(θ) in other materials that support the microbubble model. The first measurement by Cummins *et al.*[38] in salol showed that I(θ) decreased too rapidly with scattering angle to be fit by the Ornstein-Zernike theory, but could be reasonably described by Mie theory. In this thesis we have reached the same conclusion in our measurement of I(θ) in succinonitrile. Mesquita has recently measured I(θ) in naphthalene saturated with 1 atm of argon and has seen a reproducible peak in I(θ) at 50° which is highly indicative of Mie theory. We believe that these three measurements provide sufficient contrary evidence to the measurement by Steininger and Bilgram[33] to justify questioning its correctness.

It has also been suggested that there may be more than one diffusive scattering phenomenon involved. Mazur and Keizer[51], and Vesenka and Yeh[42], have noted that the bubble sizes obtained in the experiments by the ETH group[18,19,28,32] on the c axis of the ice-water system are considerably smaller than for all the other systems studied. This observation has led them to conjecture that there might be two different scattering phenomena involved, one for the c face of ice, and microbubbles for all other systems. We note however that the observation of the "lift off layer"[32] and the $1/v_g$ dependence of the thickness of the scattering layer,[32] along with the fit of Mesquita *et al.*[44], using Mie theory, to the "I vs Γ " onset data of Böni *et al.*[28] (see Fig. 1.3) seem to suggest that the phenomenon present in the ice-water system is also microbubbles. We believe that the reason for the small bubble size in the experiments of the ETH group[18,19,28,32] may be related to the method of sample preparation. This point is elaborated on further in section 5.3.

Lastly we note a recent computer simulation by Burke *et al.*[88] in which they performed a molecular dynamics study of a Lennard-Jones system. In this simulation large undercoolings were introduced producing growth rates of up to 80 m/s. In this study, the transition layer between the crystal and melt was <u>not</u> found to increase in

thickness during growth.[88] Furthermore, since the isothermal compressibility of a crystal is typically much smaller than that of its melt, it is difficult to see how the transition layer could have a compressibility hundreds of times larger than that of the melt. Therefore, the mesophase concept must be considered an essentially *ad. hoc.* explanation until additional evidence can be offered to support it.

If we assume the scattering to be caused by microbubbles two of the major remaining unresolved problems with the model are: (1) How does bubble nucleation occur, and (2) What determines the initial radius at the onset of scattering? These two problems, which are probably related, are addressed below.

5.2. The Nucleation Problem

The theory of homogenous nucleation[2] (discussed in Sec. 2.2.1) predicts that J, the number of bubbles of radius R nucleated per sec cm^2 is given by

$$J = A\, e^{-\Delta F_c/k_B T} \tag{5.1}$$

where the prefactor A depends on various material parameters and is typically $\sim 10^{32}$. The free energy barrier height ΔF_c for formation of a bubble of critical radius R_c is given by

$$\Delta F_c = \frac{4}{3}\pi\sigma R_c^2 = \frac{16\pi\sigma^3}{3(P_g - P_l)^2} \tag{5.2}$$

where σ is the interfacial tension, P_g is the gas pressure inside the bubble and P_l is the hydrostatic pressure.

In salol, for bubbles of radius $\sim 1\mu m$ with $\sigma = 20$ dynes/cm^2, $\Delta F_c/kT \sim 2 \times 10^7$, and we find from Eqs. 5.1 and 5.2 $J \sim 10^{32} \times e^{-2\times10^7} \sim 10^{-9\times10^6}$. Thus, homogeneous nucleation theory essentially predicts no nucleation. As has been noted in Sec 2.21, Wilcox and Kuo[2] estimate that an air bubble nucleation rate of 1/cm^3 sec in naphthalene would require a supersaturation of 380 atm, and in water, 1720 atm. Various models of heterogeneous nucleation in the presence of solid surfaces[12,15]

suggest that ΔF_c could be reduced by at most two orders of magnitude, leaving the theoretical nucleation rate still unobservably small at small supersaturations. It was this argument that Bilgram discussed in his 1987 review article[27] in which he rejected the microbubble model.

In spite of the depressingly small nucleation rates predicted by homogeneous nucleation theory, however, the nucleation of gas bubbles during crystal growth is actually a well-established phenomenon which has been known for many years. In 1973, Wilcox and Kuo[2] summarized the extensive literature on the observation of the generation and trapping of gas bubbles in melt-grown crystals (see sec 1.1 for some examples from this review). They noted that bubble formation during the freezing of water is particularly well known, and that in 1870 Bunsen had obtained bubble-free ice for the first time by directional freezing downward of water boiled in the tube and then sealed to exclude air. The capture of gas bubbles during solidification of both water and salol has been observed and photographed extensively in the USSR by Geguzin and Dzuba.[89] Gas bubble trapping during crystal growth is also an important technical problem since it leads to voids and imperfections in crystals.

An important clue to the effect of crystal surfaces on gas bubble nucleation was found by Hemmingsen and his coworkers.[16,90] They studied bubble nucleation in water equilibrated with various gases at high pressure and then decompressed to atmospheric pressure. No nucleation was observed for initial pressures below 190 atm for N_2, or 300 atm for He, but massive nucleation rates were observed for 20-30 atmospheres higher supersaturation.

When the water was first saturated with succinic acid or potassium nitrate and cooled to produce crystalline precipitates, it was found that the gaseous supersaturation threshold for bubble nucleation on the crystals was far lower than the value required for nucleation in the bulk fluid or on the glass-liquid interface. For succinic acid, the threshold was found to be less than 5 atm. It therefore seems that the free energy

barrier required to nucleate gas bubbles on the surface of a crystal is enormously decreased relative to the bulk value $\Delta F = \frac{4}{3}\pi\sigma R_c^2$. The mechanism for this effect is unknown, although Hemmingsen discussed the possible role of pits or cracks on grain boundaries as probable nucleation centers. We therefore conclude that heterogeneous nucleation of bubbles on the advancing crystal-melt interface explains how bubbles occur, even though the rate predicted by heterogeneous nucleation theory is negligible.

5.3. Selection of the Bubble Size at Onset

If we now accept that the scattering seen in all materials is caused by bubbles, a further problem concerns the observation that for a given material and growth velocity, the bubble size at onset R_o is fairly reproducible, for most samples $R_o \sim 1\mu m$, but for the ice water experiments performed by the ETH group[18,19,28,32] $R_o \sim 1/40^{th}$ of that size, $R_o \sim 25nm$.

There have been several suggestions put forth as possible size selection mechanisms. Ladeira and Mesquita[46] have suggested that the critical bubble radius R_o given by Eq. 2.83 must be small enough to avoid capture by the advancing interface. However, our recent observations of bubble capture in salol after prolonged growth suggest that the capture mechanism sets an upper limit to bubble size ~ 100 times larger than the observed onset value. Another possibility,[46] involves a balance between the various forces acting on the bubble once it has been created. But the increase in onset radius with growth velocity predicted by this model has not generally been observed

A mechanism which may well be crucial in determining the onset size is the crossing of a threshold for heterogeneous nucleation. Suppose that the (still unspecified) heterogeneous nucleation mechanism reduces the free energy of bubble formation from $\Delta F = \frac{4}{3}\pi\sigma R_c^2$ to $\Delta F = \phi\frac{4}{3}\pi\sigma R_c^2$ where $\phi << 1$, and that onset requires that the

nucleation rate J reach a minimum observable value of, e.g., $J=10^3$/sec cm^3, or $J=1$/sec mm^3. Further, suppose that for salol $\phi = 3.3 \times 10^{-6}$ so that the nucleation rate of Eq. 5.1, for $R = 1\ \mu$m, would be 10^3/sec cm^3.

As growth proceeds and the dissolved gas concentration at the interface increases, the minimum size for a non-collapsing bubble decreases following Eq. 2.83, and when R_c reaches 1μm, the nucleation rate would be observable. Note, however, that when R_c is 2μm, $J \sim 10^{-84}$. Therefore, no bubbles will appear until R_c is very close to 1 μm so that the combined effects of Eq. 2.83 and 5.1 can provide a very tight restriction on the initial bubble size. The nucleation rate equation would then provide the required size selection mechanism.

Indirect evidence supporting this explanation was provided by a recent nucleation study by Cumming, Wiltzius and Bates.[91] Off-critical mixed polymer melts quenched into the two-phase coexistence region produced nucleation of highly monodisperse spherical droplets of the minority phase (polydispersity $< 3\%$) which subsequently grew with time. This remarkable initial monodispersity presumably reflects the extreme dependence of nucleation rate on droplet size.

This mechanism certainly explains the reasonably narrow size distribution of bubbles nucleated at the interface. However, further key questions to be answered are what are the factors that determine this threshold, and what role the dynamics of the gas buildup plays in the process.

In experiments on the ice water system at the University of California Davis[41-43] and by the ETH group[18,19,28,32] vastly differing bubble sizes have been reported. Thus, it is instructive to look more closely at these experiments to understand the reason for this difference. It is possible that the key to the origin of the small bubble size first seen in the ETH group's[18,19,28,32] experiments may lie in the method of sample preparation. Their procedure is described in Ref. 19. It is stated that the water is circulated through a Millipore system consisting of an organic adsorption filter, an

ion exchanger and a mechanical filter with a 0.22 μm Millitube cartridge, until the resistivity of the water is below 10^{-7} Ω cm^{-1} at 25°C. This water is then used to make the seed crystal, and sample which is subsequently multiply zone refined. This procedure will indeed produce very pure water, but will probably not eliminate dissolved gases very efficiently. Thus, it is quite likely that a sample prepared this way (i.e. with deionized water) will contain more gas than a sample that has been multiply distilled. Further, our experiments along with those of Laherrere *et al.*[47,48] suggest that samples with a higher initial gas concentration C_o produce smaller bubbles. As has been mentioned in Sec 4.2.3 this effect can be explained by assuming that the rapid buildup of gases in samples that have a high C_o cause the concentration at the interface to change so rapidly that it surpasses the natural nucleation threshold and the bubbles form at a higher interfacial gas concentration and thus, via Eq 2.83, with a smaller radius.

The cleanliness of the sample may also be a contributing factor. It is a well known fact that if all sources of nucleation sites are removed or minimized then liquids can withstand large supersaturation of gases before bubbles will nucleate. A related phenomenon is that of explosive boiling[2] where a liquid is superheated past its boiling point but will not nucleate into a gas phase because of the unavailability of nucleation sites. Eventually the elevated threshold for nucleation is reached and the liquid explodes violently into the gas phase. One can imagine that as a sample is progressively cleaned its threshold concentration for heterogeneous nucleation C_N will rise until a state is reached where no sites are available, and C_N will equal the threshold for homogeneous nucleation. Wilcox and Kuo[2] have calculated both the necessary supersaturation and the critical radius for homogeneous nucleation of air in water. The critical radius is ~ 10 Å. And thus even the experiments of the ETH group[18,19,28,32] are still far in the heterogeneous regime. If we compare the ice water experiments of Brown *et al.*[41] with those of the ETH group[18,19,28,32] , Brown *et al.*[41] typically observe an onset

radius of ~ 1 μm where as the ETH group[18,19,28,32] sees an onset radius of ~ 25 nm. The ETH group impose strict criteria on each sample before data is taken. These include an absence of dust in the water and an absence of bright spots caused by dust on the interface. However in Brown *et al.*[41] even though the samples are triply distilled, a region of the interface has to be chosen that is free of dust to perform the experiment. This implies that heterogeneous nucleation sites are pervasive on the interface. Thus, the combination of a lower initial gas concentration with an environment more favorable to heterogeneous nucleation seems to yield a larger bubble size. In a subsequent publication of the Davis group, Vesenka and Yeh[42] note a decrease in bubble size (~ 50 – 75 nm) when the purification apparatus is moved inside a helium filled work box in which the sample can be kept dust free. In the same publication Vesenka and Yeh inject the sample with helium, a procedure that will surely increase the background concentration of gas but also probably increase the amount of small particulate impurities. A large increase in scattering intensity but no decrease in bubble size is seen. Thus, a large gas concentration alone cannot yield a small onset radius if an interface favorable to nucleation prevents the gas concentration from building up too much.

Thus, to summarize, the uniquely small bubble radius it is possible to observe in the ice water system is probably a consequence of the ability to apply rigorous purification procedures (i.e. filtering, passing through ion exchange columns) to the preparation of sample without having to resort to distillation which removes gas.

REFERENCES

1 M. Blander and J.L. Katz, AIChE. J. 21, 833 (1975).

2 W.R. Wilcox and V.H.S. Kuo, J. Cryst. Growth 19, 221 (1973).

3 H.E.C. Powers, Nature 182, 715 (1958).

4 J.T.A. Pollock, J. Mat. Sci 7, 631 (1972).

5 K. Nassau and A. M. Broyer, J. App. Phys. 33, 3064 (1962).

6 K. Sugii, H. Iwasaki, and S. Miyazawa, J. Crystal Growth 10, 127 (1971).

7 M. Volmer and A. Weber, Z. Phys. Chem.,119, 277 (1926).

8 R. Becker and W. Döring, Ann. Phys. 24, 719 (1935).

9 J. Frenkel, "Kinetic Theory of Liquids" (Dover Publications, Inc., New York) Chapter VII (1955).

10 J.L. Katz and M. Blander, J. Coll. Int. Sci. 42, 496 (1973).

11 J. Fisher, J. Appl. Phys. 19, 1062 (1948).

12 G.R. Moore, A. I. CH. E. Journal 5 458 (1958).

13 R. E. Apfel, J. Chem. Phys. 54 62 (1971).

14 R. Cole, Adv. in Heat Transfer 10, 85 (1974).

15 M. Blander, Adv. Coll. Int. Sci. 10, 1 (1979).

16 W.A. Gerth and E.A. Hemmingsen, J. Coll. Interf. Sci. 74, 80 (1980).

17 H. Guttinger, J.H. Bilgram, E. Serrallach and W. Kanzig, Helv. Physica Acta 48, 399 (1975).

18 J.H. Bilgram, H. Guttinger and W. Kanzig, Phys. Rev. Lett. 40, 1394 (1978).

19 H. Guttinger, J.H. Bilgram and W. Kanzig, J. Phys. Chem. Solids 40, 55 (1979).

20 J.H. Bilgram and P. Boni, in: *Light Scattering in Liquids and Macromolecular Solutions*, edited by V. DeGiorgio, M. Corti and M. Giglio (Plenum, NY 1980) p. 203.

21 B. Zysset, P. Boni and J.H. Bilgram, Helv. Phys. Acta 54, 265 (1981).

22 J.H. Bilgram, in: *Nonlinear Phenomena at Phase Transitions and Instabilities*, edited by T. Riste (Plenum, NY 1982) p. 343.

23 U. Durig and J.H. Bilgram, in: *Nonlinear Phenomena at Phase Transitions and Instabilities* edited by T. Riste (Plenum, NY 1982) p. 371.

24 J.H. Bilgram, Ann. N.Y. Acad. Sci. 404, 335 (1983) (Proc. 4th Int'l Conf. on Physico-Chemical Hydrodynamics), edited by R. Pfeffer.

25 J.H. Bilgram, Naturwissenschaften 69, 472 (1982).

26 J.H. Bilgram and P. Boni, in: *Chemical Instabilities*, ed. by G. Nicolis and F. Baras, (D. Reidel, Dordrecht, 1984), p. 351.

27 J.H. Bilgram, Helv. Physica Acta 56, 863 (1983).

28 P. Boni, J.H. Bilgram and W. Kanzig, Phys. Rev. A 28 , 2953 (1983).

29 U. Durig, J.H. Bilgram and W. Kanzig, Phys. Rev. B 30, 946 (1984).

30 J.H. Bilgram, Physics Reports 153, 1 (1987).

31 P. Halter and J. Bilgram, Helv. Phys. Acta 61, 185 (1988).

32 P.U. Halter, J.H. Bilgram and W. Kanzig, J. Chem. Phys.89, 2622 (1988).

33 R. Steininger and J. Bilgram, Helv. Phys. Acta 62, 215 (1989); J. Cryst. Growth 99, 98 (1990) (Proc. ICCG-9).

34 J.H. Bilgram and R. Steininger, J. Cryst. Growth 99, 30 (1990) (Proc. ICCG-9).

35 R. Steininger and J.H. Bilgram, Proc. 4th Nat. Seminar on Crystal Growth, Mysore, Aug. 1989 (World Scientific, Singapore - in press).

36 O.N. Mesquita, D.G. Neal, M. Copic and H.Z. Cummins, Phys. Rev. B 29, 2846 (1984).

37 O.N. Mesquita and H.Z. Cummins, Physico-Chemical Hydrodynamics 5, 389 (1984).

38 H.Z. Cummins, G. Livescu, H. Chou and M.R. Srinivasan, Solid State Commun. 60, 857 (1986).

39 G. Livescu, M.R. Srinivasan, H. Chou, H.Z. Cummins and O. Mesquita, Phys. Rev. A 36, 2293 (1987).

40 L. Williams, M.R. Srinivasan and H.Z. Cummins, Phys. Rev. Lett. 64, 1526 (1990).

41 R.A. Brown, J. Keizer, U. Stelger and Y. Yeh, J. Phys. Chem. 87, 4135 (1983).

42 J.P. Vesenka and Y. Yeh, Phys. Rev. A 38, 5310 (1988).

43 J.P. Vesenka and Y. Yeh, Bull. Am. Phys. Soc. 32, 711 (1987); 33, 781 (1988): PhD Thesis, J Vensenka University of California Davis (1989).

44 O.N. Mesquita, L.O. Ladeira, I. Gontijo, A.G. Oliveira and G.A. Barbosa, Phys. Rev. B 38, 1550 (1988).

45 O.N. Mesquita and L.O. Ladeira, "On the Nature of the Dynamic Light Scattering at the Growing Ice-Water Interface" (1988 - unpublished).

46 L.O. Ladeira and O.N. Mesquita "Laser Light Beating Spectroscopic Measurements at Growing Crystal-Melt Interfaces" (1989 - unpublished).

47 J-M. Laherrere, H. Savary, R. Mellet and J-C. Toledano, Phys. Rev. A 42, 1142 (1990).

48 J-M. Laherrere, R. Mellet, H. Savary, C. Licoppe, J.F. Scott, and J-C. Toledano, Phys. Rev. A 42, 3634 (1990).

49 J-M. Laherrere, H. Savary, R. Mellet and J-C. Toledano (unpublished). ; J.M. Laherrere, Thesis, University of Paris VI (1990).

50 J. Keizer, P. Mazur and T. Morita, Phys. Rev. A 32, 2944 (1985).

51 P. Mazur and J. Keizer, Phys. Rev. A 38, 5267 (1988).

52 P. Mazur and J. Keizer, J. Statistical Physics 57, 497 (1989).

53 W.H. van Saarloos and G. H. Gilmer, Phys. Rev. B 33, 4927 (1986).

54 H. Z. Cummins and H. L. Swinney in:*Progress in Optics*, edited by. E. Wolf (North-Holland 1970) 8, 133.

55 *Photon Correlation and Light Beateating Spectroscopy*, edited by H. Z. Cummins and E. R. Pike, Nato Advanced Institute Series, (Plenum Press 1974).

56 *Photon Correlation Spectroscopy and Velocimetry*, edited by E. R. Pike and H. Z. Cummins Nato Advanced Institute Series, (Plenum Press 1974).

57 *Laser Light Scattering*, by B. Chu (Academic Press, New York 1974)

58 *Dynamic Light Scattering*, by B. J. Berne and R. Pecora (John Wiley and Sons Inc. 1976)

59 *Introduction to Fluid Dynamics*, by G. K. Batchelor (Cambridge University Press 1985)

60 D. E. Koppel, J. Chem. Phys. 57, 4814 (1972).

61 L. P. Kadenoff and J. Swift, Phys. Rev. 166, 89 (1968)

62 G. Mie, Ann. Physik 25 377 (1908).

63 *Electromagnetic Theory*, by J. A. Stratton, (McGraw-Hill, New York 1941).

64 *Light Scattering by Small Particles*, by H. C. van de Hulst (Wiley, New York 1957).

65 L. S. Ornstein and F. Zernike, Proc Akad. Sci. 17 793 (1914).

66 F. Zernike, Proc. Acad. Sci. 18 1520 (1916).

67 H. Z. Cummins in *International School of Physics "Enrico Fermi Proceeding"* XL course (Academic Press, 1969) 247.

68 R. D. Mountain Journ. Res. Natl. Bur. Std. 70A, 207 (1966).

69 L. Landau and G. Placzek, Z. Phys. Sowjet-Union 5, 172 (1934).

70 H. Z. Cummins and R. W. Gammon, J. Chem. Phys. 44 2785 (1966).

71 *Introduction to Phase Transitions and Critical Phenomena*, by H. E. Stanley (Oxford University Press 1971).

72 H. Z. Cummins in *Proceedings of the International School of Physics "Enrico Fermi"* edited by M. Green LI course (Academic Press 1972) 380.

73 C. A. Ward, A. Balarishnan and F. C. Hooper, Trans. ASME J. of Basic Eng. 90, 695 (1970).

74 J. P. Hirth, G. M. Pound and G. R. St. Pierre Met. Trans. 1, 939 (1970).

75 W. M. Ketcham and P. V. Hobbs, Phil. Mag. 19 1161 (1969).

76 P.S. Epstein and M.S. Plesset, J. Chem. Phys. 18, 1505 (1950).

77 L. A. Crum, Appl. Sci. Re. 38, 101 (1982).

78 F. E. Fox and K. F. Herzfeld, J. Acoust. Soc. Amer. 26, 985 (1954).

79 V. A. Akulichev, Sov. Phys. Acou. 12, 144 (1966).

80 M. G. Sirotyuk, SovPhys. Acou. 16, 237 (1970).

81 E. N. Harvey, K. K. Barnes, W. D. McElroy, A. H. Whiely, D. C. Pease and K. W. Cooper, J. Cell Comp. Physiol. 24, 1 (1944).

82 A.A. Chernov and D.E. Temkin, in: *Current Topics in Material Science*, Vol. 2, edited by E. Kaldis (North Holland, 1977), p. 4.

83 E.T. Chen, R.N. Barnett and U. Landman, Phys. Rev. B 40, 924 (1989), and references 324-327 in Ref 30

84 J. H. Bilgram, U. Durig, M. Wachter and P. Seilers, J. Crystal Growth 57, 1 (1982).

85 M. Awal, PhD. Thesis, City College of the City University of New York, N.Y. (1983)

86 O. Mesquita, PhD. Thesis, City College of the City University of New York, N.Y. (1984).

87 R. Pohl, J. Appl. Phys. 25 1170 (1954).

88 E. Burke, J.Q. Broughton and G.H. Gilmer, J. Chem. Phys. 89, 1030 (1988).

89 Ya. E. Geguzin and A.S. Dzuba, J. Cryst. Growth 52, 337 (1981).

90 E.A. Hemmingsen, J. Appl. Phys. 46, 213 (1975); Nature 267, 141 (1977).

91 A. Cumming, P. Wiltzius and F.S. Bates, Phys. Rev. Lett. 65, 863 (1990).